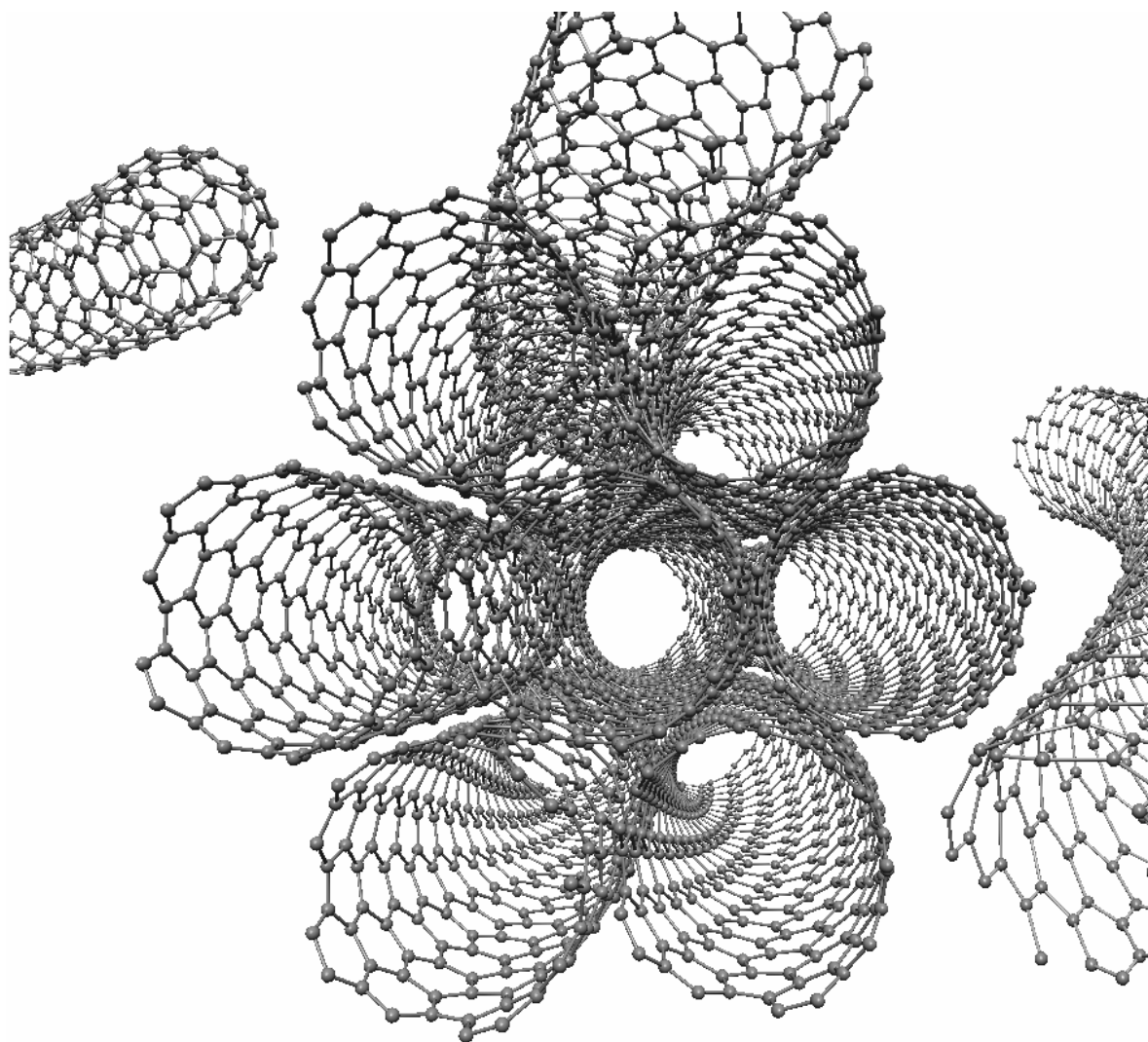


A Study of the Dispersion and Debundling of Single Walled Carbon Nanotubes



Physics and Chemistry of Advanced Materials

Trinity College Dublin



Table of Contents

ABSTRACT	1
INTRODUCTION	1
LITERATURE REVIEW	5
EXPERIMENTAL METHODS	8
<i>Dispersion preparation</i>	8
<i>UV-vis absorption measurements</i>	9
<i>NIR-Photoluminescence</i>	9
<i>Atomic Force Microscopy</i>	10
RESULTS AND DISCUSSION	11
CONCLUSIONS	29
APPENDIX	31
Appendix 1	31
1.01 Structure Assignment of Optical Spectra	31
Appendix 2	32
2.01 SWNT in NMP, smoothed and differentiated UV-vis absorption spectra	32
2.02 SWNT in SDBS, smoothed and differentiated UV-vis absorption spectra	32
Appendix 3	33
3.01 NIR-PL Map, SWNT in SDBS, Sample F (0.016 mg/mL)	33
Appendix 4	34
4.01 AFM images, SWNT in NMP, series 2	34
4.02 AFM images, SWNT in SDBS, series 2	35
4.03 Histograms for bundle diameter change with concentration, SWNT in NMP	36
4.04 Histograms for bundle diameter change with concentration, SWNT in SDBS	37
4.05 Individual and bundle mean nanotube lengths	38
Appendix 5	39
5.01 DWNT in NMP concentration behaviour	39
5.02 DWNT in SDBS concentration behaviour	39
Appendix 6	40
6.03 Future Work	40
REFERENCES	41

Abstract

This study has shown that high quality dispersions of individual single walled carbon nanotubes (HiPCO) are possible using relatively mild sonication and mild centrifugation in both the amide solvent *N*-methyl-2-pyrrolidone (NMP) and solutions of the aqueous surfactant sodium dodecyl benzenesulfonate (SDBS); a ratio of five parts surfactant to one part nanotube powder was used. This study shows that increasing the sonication energy in the SDBS system holding all other parameters constant gives better initial break-up of large aggregates. AFM data from drop-cast samples indicates number fractions of individual nanotubes of almost 85% with peak number density $\sim 3 \times 10^{19} \text{ m}^{-3}$. The NMP dispersions have shown a lower peak number fraction of individuals at $\sim 30\%$ with a peak number density $\sim 7 \times 10^{17} \text{ m}^{-3}$. The AFM data also shows saturation of the root mean square diameter at a value of approximately 3 nm at low concentrations in NMP. The SDBS system shows a well defined minimum of about 1 nm in this parameter, at the same concentration where the number fraction and number density of individual nanotubes are maximised.

Near infrared photoluminescence measurements have confirmed the presence of significant populations of individual nanotubes in both dispersion systems. This spectroscopic analysis of the emission intensity from the liquid phase dispersions agrees reasonably well with AFM data in the case of NMP but has shown a deviation at low concentration in the case of the surfactant dispersion. The PL intensity at low concentrations from SDBS samples, which relates directly to the number density of individual nanotubes, appears to be excessively high relative data derived from AFM. This can be explained by a time dependent rebundling effect, with due consideration to the preparation procedure followed. It is suggested that the low nanotube concentrations, with correspondingly low surfactant concentrations, may have irreversible surfactant desorption that promotes the rebundling of individual nanotubes.

Further inspection of the AFM data allows a crude analysis of the variation with nanotube concentration of bundle length and volume. This analysis allows us to show that for the NMP dispersions, the equilibrium volume of solvent per bundle ($V_{\text{solvent, eq}}$) is slightly lower than the volume of a sphere defined by the average bundle length. In the case of the SDBS dispersion, $V_{\text{solvent, eq}}$ is two orders of magnitude smaller than the pervaded volume of bundle. This means that especially for the SDBS dispersions, there is a high probability of collisions occurring between the bundles and this may lend further support to the feature of rebundling observed in low concentrations. It is possible that the higher number density of individual nanotubes compared to those in NMP, and the observed very close bundle proximities, is due to a greater efficacy of debundling under sonication with an overall system instability leading to re-aggregation over time. It is also possible to derive the molar mass of individual nanotubes and this is shown to be $9.7 (\pm$

$0.4) \times 10^5$ g/mol based on data from NMP dispersions and $7.0 (\pm 0.4) \times 10^5$ g/mol for the SDBS system.

This study also aimed to conduct a full concentration dependent characterisation of double walled nanotubes in both NMP and SDBS. Due to time limitations this was not possible but the observance of very long nanotube bundles of small diameter from NMP samples indicates great scope for future work.

Introduction

Carbon nanotubes are tubular allotropes of carbon that have received much scrutiny since first being observed in 1991 by S. Iijima in the soot of arc discharge produced fullerenes.¹ As a first visualisation, carbon nanotubes can be viewed as linear elongations of the C₆₀ species, the fullerene or “buckyball”, resulting in rope-like structures. Indeed, some early literature refers to these entities as “graphene tubules based on C₆₀”.² An alternative visualisation is that of seamlessly rolling up a graphene sheet composed of a hexagonal network of sp² hybridised carbon atoms to yield a single walled nanotube (SWNT). These SWNT structures have high aspect ratios with nanometre diameters typically in the range 0.4 - 1.4nm (approx 10-40 atoms) and end to end lengths ranging up to several microns.³ A series of concentrically centred tubes yields double and multi-walled nanotubes, with abbreviations of DWNT and MWNT.

Collectively, these nanotube species have unique physical and chemical properties. For instance, carbon nanotubes have been shown to exhibit Young’s moduli greater than 1TPa with mechanical strengths of ~60GPa, far in excess of the strongest materials hitherto known to humankind.⁴ The form of the sp² hybridised carbon network allows for an effective one dimensional structure with resistance-free ballistic transport along the length of the tube – this allows extreme current densities of ~100MA/cm² to be supported⁵. Note that the electrical conductivity is dictated by the way in which the tubes are rolled up with tubes being either metallic or semiconducting. Nanotubes also have excellent phonon conductivity with theoretical thermal conductivities, at room temperature, of about 6000W/mK⁶.

In terms of direct device applications, CNTs have already found their way into scanning probe microscopy as high spatial resolution tips for atomic force microscopy (AFM) – their strength and narrow radius being exploited. It has been suggested that they may even be useful as hydrogen storage media in future fuel cell technology⁷. A more promising area of research lies with material reinforcement via the integration of CNTs into polymer matrices. A wide range of polymeric systems have been shown to have enhanced mechanical properties as a result of introducing relatively small quantities of CNTs; recently SWNTs have been shown to increase the Young’s modulus of the semi-crystalline poly-vinyl acrylate (PVA) by a factor of three merely by use of 0.1vol% of nanotube.⁸ The electronics industry is currently examining ways of utilising the field emission properties of CNTs to develop next generation visual display units; such units may use controlled field emission from a nanotube coated anode to illuminate phosphors yielding bright displays that will have wide viewing angles⁷. The semiconductor industry is also looking at the possibility of using CNTs as an alternative to the currently used copper or aluminium transistor interconnects; for the device engineer, the metallic tubes exhibiting ballistic transport together with

excellent mechanical strength are ideal candidates, provided the high contact resistance can be overcome.⁹

Many applications, including all of those above, rely on varying degrees of specificity in nanotube type, diameter, length and electrical character. In particular, the electronic structure of the tubes is of relevance to numerous potential applications and, more importantly, to the experimentalist. A range of spectroscopic techniques probe this electronic structure and allow quantitative analysis of a range of nanotube systems; for instance photoluminescence and UV-visible absorption spectroscopy are utilised in this work to probe nanotubes dispersed in a liquid phase. The electronic structure is determined by the manner in which the graphene sheet is rolled. The process of rolling inherently disrupts the symmetry of planar graphene, thereby altering the electronic band structure and resulting in either metallic, semi-metallic or semiconducting nanotubes. Thus, it is useful to give a brief overview of the common structure indexing system, chirality[†] and band structure together, given in Figure 1 through Figure 3.

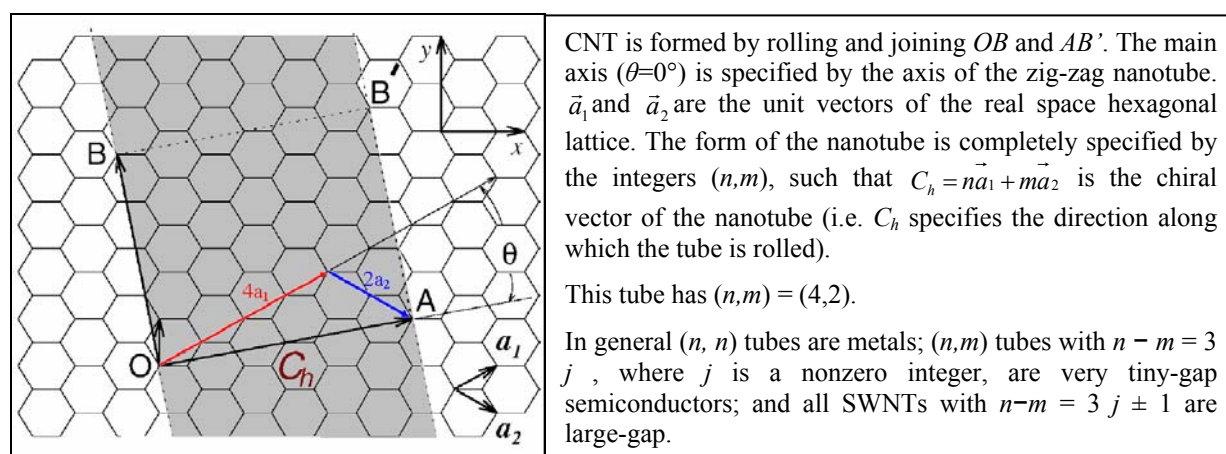


Figure 1: Unrolled lattice structure of nanotube. Image adapted from that presented by Dresselhaus et al.³

The direction along which the graphene sheet has been “rolled” directly impacts the band structure and so, from above, band structure can be linked to the chiral vector of the tube. Note, however, that the direction of the chiral vector alone is not sufficient to specify the electronic nature of small diameter tubes (diameter D near 0.4 nm). A small diameter tube has sharp curvature of the nanotube surface allowing significant interaction between the σ bonding orbitals and the delocalised π system. Also worth noting is that (n,n) tubes will always[‡] be metallic due to the symmetry of the molecule. Figure 3 below gives an illustrative plot of the electronic densities of states of three types of SWNT (note that the tiny gap (7, 1) type will be effectively metallic at room temperature due to available thermal energy).

[†] Chirality refers to the “handedness” of molecules. In particular, those structures that have non-superimposable mirror images are referred to as *chiral* while those having super-imposable mirror images are *achiral*.

[‡] This statement applies to ideal nanotubes with a defect free surface and an absence of sharp kinks along the length of the tube.

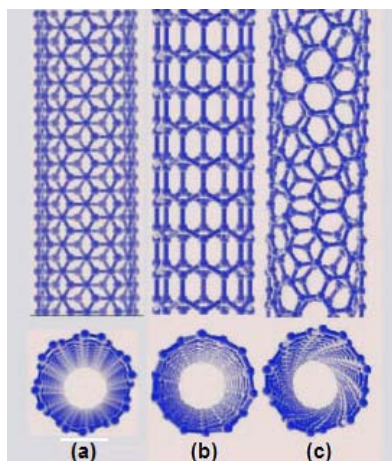


Figure 2: Schematic illustrations of (a) armchair, (b) zigzag and (c) chiral SWNTs.⁷

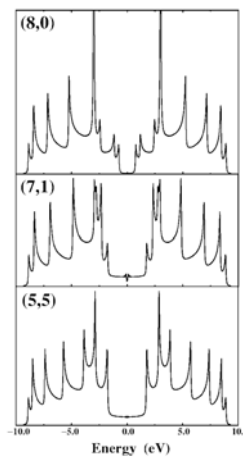


Figure 3: Electronic densities of states of various (n, m) nanotubes.³

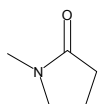
The production process for nanotubes will directly impact the distribution of chiralities, along with length and diameter distributions – this in turn dictates the suitability of the end product for the various applications mentioned earlier. Common techniques for producing SWNT and MWNT include arc discharge, laser ablation and catalytic CVD.¹⁰ Newer catalytic methods for SWNT production include High Pressure Carbon Monoxide (HiPCO[®]) and carbon monoxide disproportionation, known as CoMoCat[®]. A problem with all of these types of production techniques is that the end product is composed of large entanglements of nanotube ropes with varying degrees of residual soot and catalyst impurity. The entanglement results directly from the flexibility and very high Van der Waals surface energy of the nanotubes (quantified at about 0.5eV per nanometre length¹¹)– aggregation of the nanotubes reduces energy and so is an energetically favourable process. Also, the fact that nanotube synthesis results in a mixture of semiconducting and metallic nanotubes (roughly in a ratio of 2:1 by number for semiconducting:metallic)¹² means that separation of aggregates into individual tubes becomes even more important; this segregation is the obvious first step to future use of CNTs in electrical devices.

Several studies have shown that SWNTs can be dispersed as bundles with the use of various agents such as aqueous surfactants (see next section). A route to attaining pristine individual SWNTs is to bring about separation of the individual tubes while dispersed in the liquid phase, a phenomenon known as nanotube *debundling*. The ultimate goal is to find a solvent or binary system in which CNTs will be thermodynamically *soluble*, whereby actual solvation of individual CNTs would occur spontaneously (Gibbs free energy of mixing being negative). Work towards this objective is ongoing and this project primarily aims to quantitatively investigate sonication-assisted debundling of SWNT in suitable liquid phase systems. In particular, their behaviour in sodium dodecyl benzenesulfonate (SDBS) aqueous solutions and in the amide solvent *N*-methyl-2-

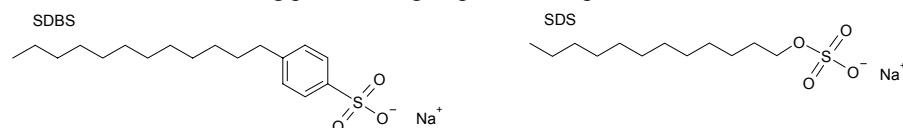
pyrrolidone (NMP) § will be compared. Obviously from a device perspective, two component systems such as that provided by the NMP are favoured over three component systems as the effects of residual dispersant (i.e. surfactant) can play havoc with the physical and chemical properties of the end product.

These two systems use very different means to facilitate nanotube dispersion. SDBS is an ionic surfactant similar in structure to sodium dodecyl sulfonate (SDS) **. Both of these surfactants have been shown to readily disperse individual carbon nanotubes if powerful sonication and ultracentrifugation are used^{11,12,14-16}; we will examine the dispersions in SDBS obtained using mild sonication and mild centrifugation. The surfactant adsorbs onto the nanotube surface, perhaps forming a micelle, with polar headgroups in contact with the water – this arrangement of surfactant allows the individual nanotubes or small bundles to stay dispersed. The NMP dispersant, as will be discussed later, is thought to rely on strong electron pair donicity which allows solvent-solute interactions to become favourable, thus improving surface coverage of the CNT surface by solvent molecules and thereby aiding debundling. We consider it useful to compare the behaviour of water/surfactant and single solvent systems as the samples deposited from these dispersions will have different scope for future applications – in particular the properties of surfactant coated nanotubes are often inferior to pristine samples. In this study we use HiPCO SWNT which are known to have a narrow diameter distribution for single tubes in the range 0.4 – 1.4 nm.¹⁷ We also aim to briefly consider DWNT dispersions in these liquid systems as a further comparison. The overall methodology involves dispersion of the nanotubes at varying concentrations with spectroscopic analysis of the liquid systems (UV-vis absorption and NIR-PL) followed by a detailed statistical analysis of bundle size based on AFM data collected from nanotubes deposited on suitable substrates.

§ NMP, is a common amide with boiling point 202°C. ¹³ It is a polar hygroscopic solvent. Below is a structure illustration:



** SDS, sodium-dodecylsulfate, is similar in structure to SDBS (also often referred to as NaDDBS). Both are classic anionic surfactants having polar head groups and non-polar tails. Below are molecular structure illustrations:



Literature review

This study examines the dispersal of CNT material in two different media, an amide solvent and an aqueous solution of surfactant. Much of the early work on nanotube dispersions centred on the surfactant-based systems – for instance Bonard et al. in 1997 used SDS to suspend nanotube aggregates as a means to assist purification by flocculation of arc-discharge produced MWNT.¹⁸ Following this, in 1998 Duesberg et al. successfully demonstrated that SDS could allow high purity SWNT (albeit with low yield) to be formed by column elution of the dispersion following ultracentrifugation.¹⁹

More recently, O'Connell et al. conducted a detailed analysis of the band gap fluorescence of individual semiconducting SWNT, again dispersed in SDS.¹¹ This study used UV-vis absorption spectroscopy to highlight the presence of individual nanotubes in the dispersions. The dispersions tested were prepared by high power treatment with a cup horn sonicator followed by ultracentrifugation ($\sim 122,000g$), the supernatant was then analysed. This work revealed the presence of sharp peaks in the absorbance and emission spectra that correspond to direct band gap transitions in the semiconducting tubes; the transitions occur between the band positions of the Van Hove singularities in the DOS, as illustrated in Figure 3. The observance of these sharp peaks is significant as it highlights the presence of individual nanotubes or very small bundles. The energy for the i th pair of transitions in semiconducting or metallic single walled nanotubes can be approximated by²⁰

$$E_{ii} = \frac{2na_{c-c}\gamma_0}{D} \quad (1)$$

where a_{c-c} is the carbon-carbon bond distance (0.144 nm)²¹, γ_0 is the carbon overlap integral ($2.45 - 3.0 \text{ eV}$)²⁰, D is the nanotube diameter and n is an integer having values $n= 3,6$ for second inter-band transitions in metallic tubes and $n= 1,2,4,5$, or 7 for first inter-band transitions in semiconducting tubes.²² Given that a relatively high percentage of tubes in any given sample will be metallic, a bundle of three or more tubes is likely to contain at least one metallic nanotube. Thus, the excitons involved in band gap transitions in semiconducting tubes are likely to be quenched in nanotube bundles – significantly, this quenching applies to both the absorption and emission spectra of a sample. Note that the use of intense sonication followed by severe centrifugation in the range $20,000 - 200,000g$ is thought to be required to obtain good dispersions of clean SWNT.¹⁶ It has been suggested elsewhere that the use of mild centrifugation for surfactant systems is insufficient to remove large bundles and hence the UV-vis absorption spectra obtained are expected to be broadened with poor definition of peak positions.²³ This approach to nanotube dispersion in surfactants has been followed in the majority of studies to date; the approach for our

study is to compare the surfactant system to an amide dispersion using significantly milder centrifugation.

Related to the optical properties of CNTs, Bachilo et al. compared experimental photoluminescence observations with computational simulations.²¹ They showed that the spin-allowed band gap emissions could be related to computational models and to Raman peaks. From this, a structure assignment of the optical spectra was obtained – further details are given in Appendix 1.01. We will use this structure assignment to label the photoluminescence maps obtained for our SWNT systems. The use of PL is of great importance to our particular study, somewhat so for deriving structural assignments but far more importantly as PL will allow direct assessment of the number density of individual nanotubes present at varying concentrations. The PL intensity will be used to assess the extent of debundling present in the systems studied, this will be discussed later. Also of note in relation to the PL spectra of semiconducting SWNTs is a recent paper by McDonald et al. suggesting that dilution of surfactant based systems promotes nanotube rebundling, resulting in quenching of the PL signal.¹² It is suggested that the PL intensity decays with first order dependence on the concentration of isolated tubes. The authors suggest that surfactant desorption from the nanotube surface is rate limiting in the overall process of nanotube rebundling. As mentioned earlier, bundles containing metallic tubes will have PL signal quenching and so this study may suggest a need to conduct PL measurements in a timely fashion after sample preparation. It is stressed, however, that this result presented in this particular paper may not be directly transferable to this study as the authors do not specify the actual concentration of individual nanotubes present while conducting the time-dependence study; therefore it is included as food for thought.

As regards dispersions in organic solvents, the alkyl amides collectively have shown promising results. Ausman et al. focused on the UV-vis absorption spectra of SWNT in NMP and *N,N*-dimethyl-formamide (DMF), suggesting that high electron pair donicity and low hydrogen bond parameters lead to good dispersion of the strongly non-polar nanotubes.²⁴ This view was reasserted by Furtado et al. who also derived a statistical distribution of nanotube diameters in these two solvents.²⁵ Landi et al. also concurred with these conditions, finding that *N,N*-dimethylacetamide (DMA) was optimum for dispersal of *acid-purified* arc-discharge SWNTs in the solvents tested.²⁰ The emphasis is included to highlight the fact that the chemical and physical treatment of the raw CNT soot prior to dispersal in a solvent is of importance. The effects of features such as chirality, length, surface defects, side-wall functionalisation and residual impurity are significant when determining optimal dispersion conditions. As such, each study should carefully state the source of nanotubes used, any additional processing carried out and the exact

sample preparation procedure used. The results obtained by Landi and others are specific to the type of nanotubes used under their given sets of conditions.

In a very recent study, Giordani et al. examined the large scale debundling of HiPCO SWNT in NMP.¹⁷ The preparation procedure used involved a relatively short duration of point probe sonication followed by four hours low power sonication in a sonic bath. The key difference between the method adopted and that of others^{12,20,24,25} was the use of mild centrifugation at ~4000g. Their study found that stable dispersions of nanotubes formed with a strong dependence of bundle diameter on the post-centrifugation nanotube concentration – saturation of the root mean square bundle diameter at ~2nm was observed below about 0.004mg/mL. Their study found measurable, though relatively weak, PL intensity from NMP samples; importantly the study showed strong concentration dependence of the PL intensity that reflected AFM analysis of samples deposited on silicon. Their study used the fact that the PL intensity obtained is proportional to the number density of individual single walled nanotubes which can then be compared to the diameter counts obtained from drop-cast AFM samples. Their study demonstrates excellent nanotube debundling in NMP and sets out an analytical framework. In this study, we will adapt as necessary the sample preparation procedures and analytic techniques used by Giordani et al.

Experimental Methods

In this study, sonication assisted dispersions were prepared at a range of concentrations for single and double walled nanotubes. We aimed to directly compare the various systems under examination and so we used similar sample preparation procedures for each sample set.

The general approach was to prepare a known concentration of raw carbon nanotube powder which was then agitated by sonic tip to finely disperse individual nanotubes, nanotube bundles and any impurity material present. This sample was then serially diluted with each new dilution being sonicated again. All samples were then placed in a low power sonic bath for a specified period of time before being given another short burst of acoustic energy by sonic tip. UV-vis absorption spectra were taken immediately after completion of the sonication routine with the samples then undergoing mild centrifugation. What was estimated to be the primarily homogeneous component of the resultant supernatant was carefully extracted and reanalysed with the UV-vis spectrophotometer. These dispersions were then drop-cast on appropriate substrates to allow quantitative assessment, by atomic force microscopy, of the bundle size distribution parameters as a function of concentration. The dispersions were also analysed using NIR-photoluminescence spectroscopy as a means of characterising optically active (presumably mostly individual) nanotubes in situ whilst still part of the liquid phase dispersion. What follows is a more detailed point-by-point account of the experimental procedures and techniques used in this study.

Dispersion preparation

Raw CNT powder was used as supplied by manufacturers with the SWNT (HiPCO) samples being sourced from Carbon Nanotechnologies Inc (lot no. P0288). The DWNTs used were purchased from Nanolab (lot no. CNN50-L1-5) and from Nanocyl (lot no. NFL 36.7). All powders were used as supplied with no additional purification carried out. The NMP solvent used was HPLC grade (99.9%+ purity at point of manufacture) purchased from Sigma Aldrich and used two weeks after the bottle was first opened (age of the NMP is important as this amide readily absorbs moisture from the ambient). The SDBS powder was also supplied by Sigma Aldrich.

For the NMP samples, a starting concentration of 1mg/mL of CNT powder was prepared and sonicated with a point probe tip for 2 mins at 60 kHz with 120W power (using a GEX600 ultrasonic processor). A 10mL volume of solvent was used with all samples prepared in 14mL stoppered vials– the tip was placed approx 1 cm below the surface of the liquid with no cooling system for the vial. The initial dispersion was then serially diluted to yield a range of concentrations spanning 1 to 5×10^{-4} mg/mL. After each dilution, 2 min sonic tip was applied. All samples were placed in a low power sonic bath for 4 hrs and then given a further 1 min sonic tip. The samples were then centrifuged at 5500 rpm (~ 3600 g) for 90 mins. The upper 80% of the

supernatant was extracted and placed in clean vials, with due care taken to prevent disturbing the sediment and drawing up large aggregates.

For surfactant dispersions, 250 mg of SDBS powder was dissolved in 50 mL of millipore water (with resistivity 18.2 M Ω cm) and left stirring for a minimum of 12 hrs with a stirring pellet – the use of relatively large volumes and masses helped reduce experimental error. From this stock solution, 10 mL were drawn to prepare the first high concentration dispersion – a ratio of five parts surfactant to one part CNT by mass was used. We initially used the same preparation procedure as applied to the NMP dispersions but based on experimental results, to be discussed later, we altered the preparation procedure. The power amplitude for point probe sonication was increased to 210W with the samples undergoing 5 mins sonic tip followed by 1 hr sonic bath and then a further 5 mins tip. This represents an approximately six fold increase in total energy supplied by the sonic tip, though this energy input is still considered mild compared to other published work.^{12,16,26} Due to the great increase in energy supplied, it was necessary to cool the system during sonication to prevent evaporation of water and any additional changes to the nanotube composition due to excessive thermal stress. Thus, the vial was immersed in ice-water during probe sonication.

Note that the labelling system for each dataset of 12 samples used letters A-L in order of decreasing initial concentration, henceforth this system will be used alongside actual concentration values to assist referencing but the reader should note that these letters only refer to approximate initial concentrations and bear no relevance to any one dispersion system or to the final nanotube concentration, C_{NT} .

UV-vis absorption measurements

UV-vis measurements were initially carried out on a Shimadzu UV-2401PC spectrophotometer – this apparatus was used for the NMP dispersion dataset. Subsequently, for the DWNT and SWNT surfactant systems, a Varian Cary 6000i UV-vis-NIR spectrophotometer became available and was used. All measurements were carried out in dual beam mode with a reference cuvette in place to prevent errors arising from differences in beam path length and all scans were baseline corrected – in the case of surfactant dispersions, the baseline taken was that of pure water. In general, 1 cm or 1 mm quartz or glass cuvettes were used, depending on the limits of detection of beam transmittance. To ensure consistency in results, scans were taken with both cuvettes at the concentration where a changeover was required.

NIR-Photoluminescence

NIR-PL measurements were made with an Edinburgh Instruments PL using a monochromated Xenon source and cooled InGaAs detector. The detector was cooled by evaporated liquid nitrogen to -80°C and allowed to stabilise whilst powered on for a minimum of two hours prior to any measurements being made. All spectral maps and line scans were baseline corrected.

Full emission maps were taken for samples where strong photoluminescence was expected and the peak positions used to determine the excitation wavelength for line scans taken across all samples. Due to the constraints imposed by the volume of liquid nitrogen stored in the dewar, full maps were only run once. All line scans were collected as a sum of two individual scans.

Atomic Force Microscopy

AFM analysis was carried out with a Veeco Multimode Nanoscope III in tapping mode using Si tips. This analysis required the use of clean nearly atomically flat substrates and so bare silicon pieces were used. These were cleaved from a 2.5 inch wafer and cleaned by boiling for 20 mins in a solution of one part ammonia, one part hydrogen peroxide and five parts de-ionised water. This was followed by a rinse in de-ionised water and blow drying with compressed air.

NMP samples were deposited by drop-casting immediately after centrifugation. To prevent excess material being deposited at high concentrations, the liquid was dropped and then largely withdrawn by pipette. NMP has a relatively high boiling point of 202°C¹³ and so samples were dried under vacuum at 80°C for two hours.

For the surfactant systems, it was found that straight drop casting on Si and oven drying resulted in re-aggregation of the nanotubes. This drying effect is caused by the withdrawal of the solvent and occurs when the nanotubes attempt to maximise inter-tube contacts in the absence of solvent.¹⁷ Obviously, such drying effects are a concern when deriving statistics from AFM data. In an attempt to obtain clean depositions for the surfactant-based dispersions, we tried using thin mica slivers. We also attempted to spin coat the nanotubes onto mica by dropping 20 µL of sample and spinning at 2000 rpm for 1 min. This was followed 2 mL of IPA rinse to remove excess surfactant and a further 3 min spinning. The spin coating technique, however has obvious drawbacks with the possibility that weakly adhering nanotubes bundles may be washed away by the IPA or that the actual spinning may yield a distribution of tube sizes that varies with radial distance from the centre of the mica disc. Thus, we attempted to drop cast on heated silicon substrates (maintained at 60°C) with slow withdrawal of the drop allowing the water present to evaporate readily – this method was used for the samples from which AFM-based statistics were derived.

Results and Discussion

The first step in analysing the composition of the nanotube dispersions was to examine the UV-vis absorption from before and after centrifugation. The Beer-Lambert law gives the concentration dependence of the absorbance with

$$A = \alpha Cl, \quad A = \log_{10} \left(\frac{I_0}{I} \right) \quad (2)$$

where α is the extinction coefficient, l is the path length. I and I_0 are the sample and reference transmitted intensities. The absorbance at 660 nm was used to derive the initial (subscript I) extinction coefficient before centrifugation, $\alpha_{660, I}$; this value can be derived at each concentration as both path length and initial concentration, C_I , are known. The 660 nm wavelength was chosen as it represents a strong absorption peak for typical HiPCO SWNTs.¹⁷ Assuming that the value of $\alpha_{660, I}$ at low concentration is representative of the individual nanotubes and small bundles present, one can extract the concentration of nanotubes after centrifugation, C_{NT} ; this could be done by using the values of $A_{660, F/l}$ (subscript F for *final*) and assuming that the extinction coefficient for these species is unchanged after centrifugation. However, if the extinction coefficient has significant variation over the concentration range, then it is more useful to assume that α will have the same value before and after centrifugation at each concentration. Thus, C_{NT} can be estimated by taking the initial concentration and multiplying by the ratio of absorbencies per unit length. The error in concentration will be considered negligible for later statistical analysis. With knowledge of C_{NT} , the mass fraction of aggregate material is given by

$$\chi_{agg} = \frac{C_I - C_{NT}}{C_I} \quad (3)$$

For the first set of SWNTs dispersed in NMP, it was observed that high concentration samples were composed predominantly of large aggregates with a decreasing proportion of aggregate material as concentration was reduced, tending towards no large aggregates at low concentration. Figure 4 is a set of graphs showing the variation of A_{660}/l , $\alpha_{660, I}$ and χ_{agg} as a function of initial concentration. It is also clear that the extinction coefficient rises with decreasing concentration, which would be the result of a change in the optical character of the system. This may be caused by an increase in the numbers of small bundles and individual nanotubes at low concentration. Due to an excessively large time delay in carrying out the remaining analysis on Series 1 using AFM and PL measurement, a new batch was prepared.

Series 2 of SWNT in NMP had one notable difference to Series 1, that being the age of the NMP used. For Series 1, three months old NMP, which had been stored in a closed bottle under normal atmosphere, had been used which would mean that a significant quantity of water could have been absorbed. For Series 2, fresh HPLC grade NMP taken from a two week old bottle was

used. The results of the UV-vis absorption analysis are presented in Figure 5 with the actual post-centrifugation spectra for Series 2 given later in Figure 7.

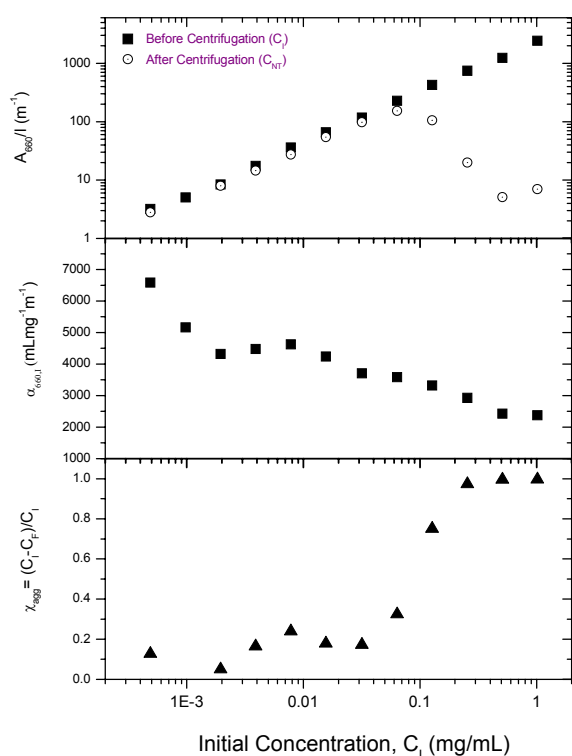


Figure 4: SWNT in NMP Series 1, absorption analysis.

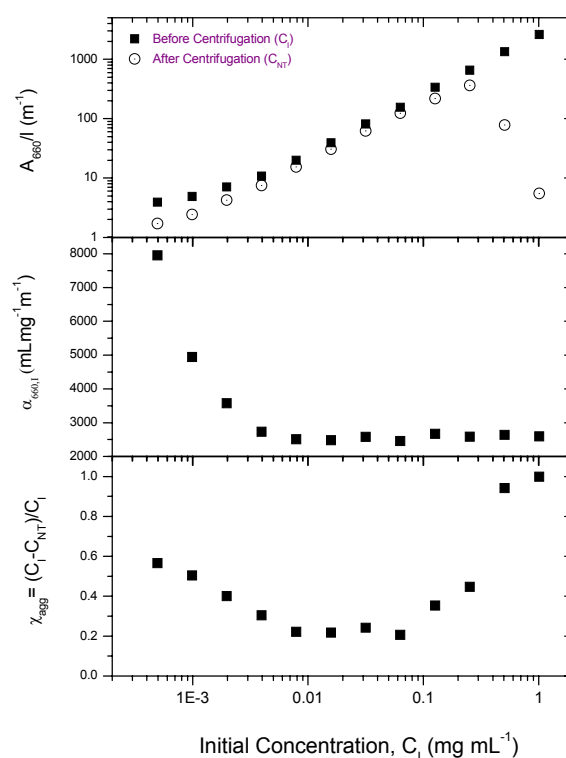


Figure 5: SWNT in NMP Series 2, absorption analysis.

For NMP Series 2, it is seen that the extinction coefficient increased at very low concentration having remained fairly constant at higher concentrations. Also of note is the NMP solvent's retention of more material at higher concentrations; evident from the trends in aggregate mass fraction. For Series 2 it does appear as though significant quantities of aggregate material were present at very low concentration, rising to above 50% aggregate – this does not appear to agree with the work carried out by Giordani et al.^{17,27} It could simply be the nature of the system that larger bundles tended to reform at very low concentration; given the work presented by others on amide dispersions this does not seem likely.^{17,20,27} At low concentration, there is a marked increase in the pre-centrifugation $\alpha_{660,l}$ in Figure 5, which is a deviation from the Beer Lambert law. It seems counter-intuitive that bigger bundles forming would cause this effect as rebundling would reduce the number of individual nanotubes present, and so reduce the number density of light scattering and optical absorption species present. It is useful to recall that C_{NT} has been derived using ratios of path-length normalised absorbencies – using this method assumed that the extinction coefficient before and after centrifugation was unchanged. It is possible that the very low concentration systems, immediately after the final sonic tip treatment, had a disproportionately large population of individual nanotubes in a state that had not established equilibrium. This effect

would be exaggerated at lower concentrations; as is observed in Figure 5 and to a lesser extent in Figure 4.

The sample preparation procedure did not allow for a significant settling period for the system, typically the natural delay between final sonic tip and UV-vis spectroscopic analysis was of the order of 10 to 20mins. The supernatant extracted after centrifugation may well have emerged in an equilibrium state with very small, stable bundles and perhaps a reduced extinction coefficient. This may explain the apparent presence of significant fractions of large aggregates at low concentration.

For the SWNT dispersed in SDBS, Series 1 was prepared using the same sonication preparation procedure as for NMP samples. Series 2 used the longer sonication procedure with ice-water cooling of the vials. Both series used a ratio of 5:1 for surfactant to CNT powder. Figure 6 below details the analysis of the UV-vis absorption for both these series (all red data points for Series 1, black for Series 2).

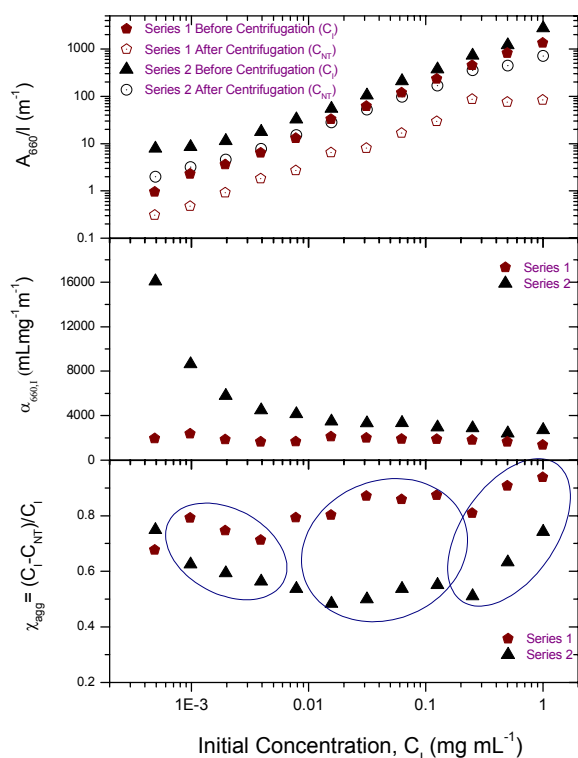


Figure 6: SWNT in SDBS, absorption analysis.

It is immediately apparent from Figure 6 that the longer sonication time had the general effect of raising the extinction coefficient. This may be indicative of a finer dispersion with more individual nanotubes being dispersed, which would be an expected result of increased sonication. Also of note is that the first series with significantly lower sonication does not show as large a rise in extinction coefficient at very low concentration – this could simply be an artefact of a possibly larger time lag between final sonication and the pre-centrifugation UV-vis analysis or due to the longer time in the sonic bath. The absorbance per unit length after centrifugation for Series 2 is

comparable to the pre-centrifugation value for Series 1, further indicating that the large bundles are broken up more effectively by increasing sonication energy. Series 2 was seen to have a significantly lower mass fraction of aggregates across the whole initial concentration range; this indicated better retention of nanotube material. It is rather interesting to note that the two systems show very similar trends for the variation of χ_{agg} as a function of initial concentration. The highlighted regions of Figure 6 indicate the high, intermediate and low concentrations regimes where the overall trends in χ_{agg} can be seen to match well; this suggests that the concentration dependence of the aggregate presence does not change with increased sonication even though there is a decrease in the population of large aggregates of nanotubes.

The UV-vis spectra taken after centrifugation were also examined in further detail. Figure 7 through Figure 9 below give the change of extinction coefficient after centrifugation as a function of excitation energy. The use of the extinction coefficient gives a representation of the absorption profile that is normalised to both concentration and path-length, thus aiding comparisons. The labelling gives estimated peak positions in the abscissa units of electron volts. To assist isolation of peaks, the line spectra were smoothed and differentiated with absorption peaks and troughs corresponding to zero points in the derivative; these plots are given in Appendices 2.01 and 2.02. The absorption peak at 660 nm, used to earlier for determining concentration, corresponds approximately to the transitions labelled at 1.89 eV. Also, if we use eqn 1 and assume a nanotube diameter of 1 nm, and $\gamma_0 = 3$ eV, then transitions near 1.7 eV are semiconductor 1-1 transitions and those near 2.6 eV are metallic 2-2 transitions.

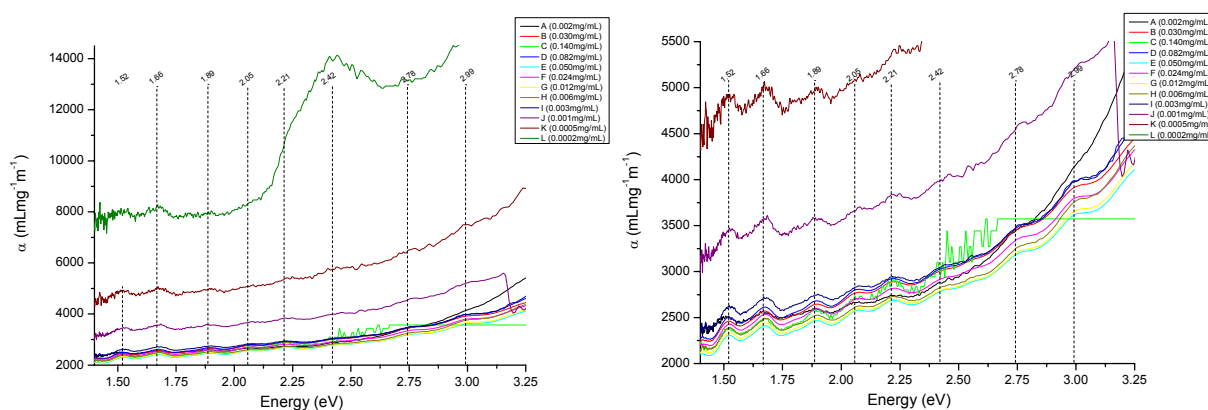


Figure 7: UV-vis absorption spectra, SWNT in NMP Series 2 (taken with Shimadzu UV-2401PC).

The NMP spectra have fairly broad features with a lot of background noise; thus a limited number of peaks have been labelled. The spectra for SDBS dispersed nanotubes have more well defined features but, more importantly, the noise in the scans for SDBS series 1 is significantly higher than that in series 2; the significant difference between these datasets being the quality of spectrometer used. The Varian Cary 6000i, with a more sensitive detector and more refined optics, had transmittance sensitivity estimated to be 10,000 times greater than the Shimadzu UV-2401PC. Thus, the noise and relative lack of well defined peaks in these spectra are likely to be due to the

spectrometer sensitivity and not the nature of the dispersing medium. This assertion is further supported by the high spectral resolutions obtained for amide dispersed HiPCO nanotubes in other studies.^{17,20,27,28}

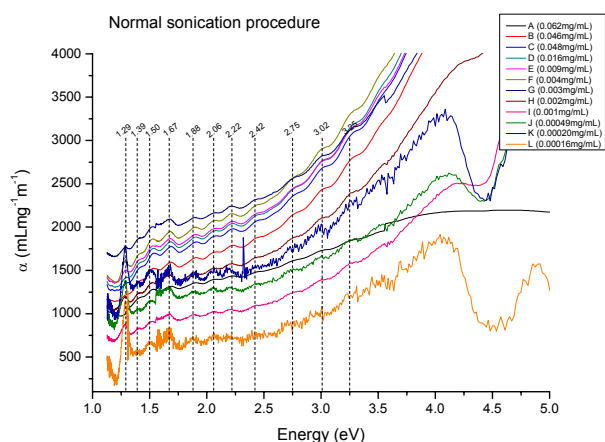


Figure 8: UV-vis absorption spectra, SWNT in SDBS Series 1 (taken with Shimadzu UV-2401PC).

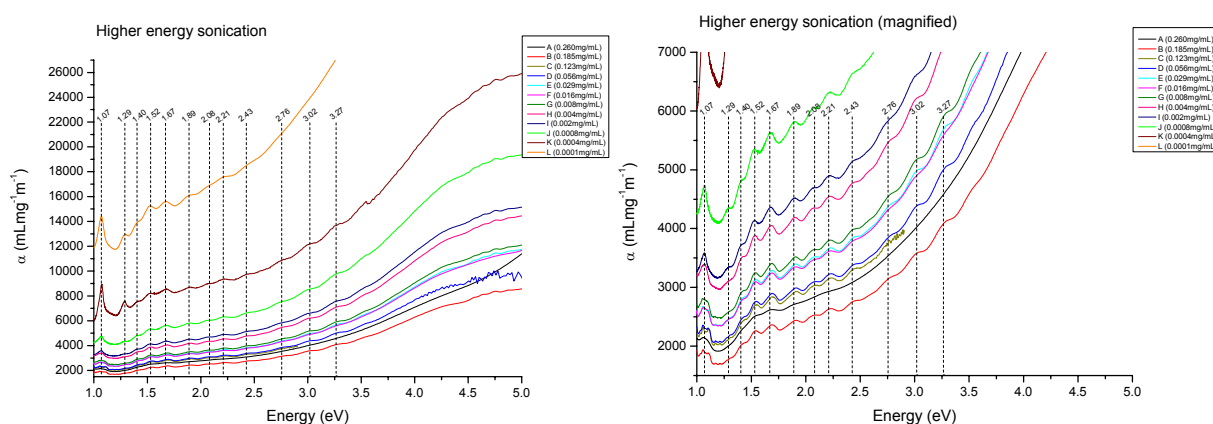


Figure 9: UV-vis absorption spectra, SWNT in SDBS Series 2 (taken with Varian Cary 6000i).

As regards the SDBS dispersions, there is good matching of the energies with no additional or missing peaks between the two types of sample preparation. Wild variations in the distribution of nanotube structure types, extensive sidewall damage or selective debundling would show up as different peak positions. Thus, we can state that increasing the sonication energy by a factor of six does not dramatically change the distribution of nanotubes, within the low to intermediate energy electronic transitions labelled; we cannot say that no change has occurred without a detailed composition breakdown. The spectral resolution appears to be better in Figure 9 for the samples with higher sonication, in agreement with other published results¹⁶, but again in our case this could be attributable to the far superior spectrophotometer used. It is clear from Figure 9 that the electronic transitions between Van Hove singularities in the density of states were well defined for the sample preparation that was used. In particular, it has shown that the use of very mild centrifugation (~3400 g) allows sharp peaks to be observed at all concentrations. This can be taken as an initial indication that the very large aggregates had been successfully removed.

Note that the photoluminescence and AFM analysis was carried out single walled nanotubes and specifically on Series 2 for both NMP and SDBS systems. All subsequent results and discussion refer to these batches

The NIR-PL measurements for SWNT NMP samples yielded emission scans of very low intensity; the relatively low intensity in NMP has been reported elsewhere¹⁷. To assist capture of emission maps for the NMP samples, the excitation monochromator width was increased from 15.0 nm to 25.0 nm while the emission width from 10.0 to 25.0 nm (the lower values were used for all SDBS samples). This has the drawback of reducing the overall sharpness of features in the maps but was seen as necessary to obtain reasonable peak amplitude. An example of a map at an intermediate concentration is given below in Figure 10. All maps and line scan data have been normalised to the same level to allow direct comparison of intensity. The reason for the poor intensity is not yet fully understood but it is likely that there is some form of charge transfer mechanism between the fluorescent semiconducting nanotubes and the surrounding NMP that is reducing the number of photons striking the detector. The main peak at excitation 825 nm, emission 1200 nm has been identified as a large scattering peak that was observed in all NMP dispersion maps.

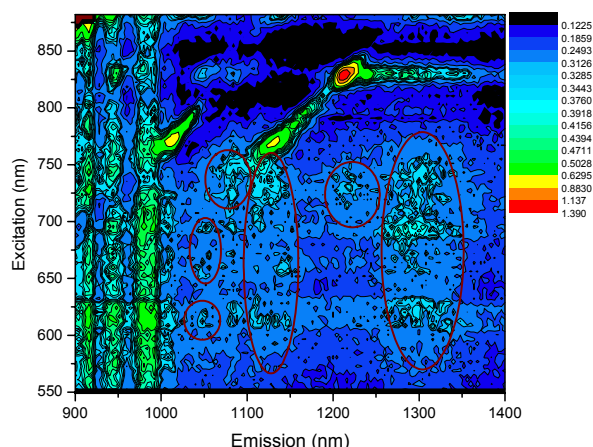


Figure 10: PL map of SWNT in NMP, Sample E (0.206 mg/mL).

Clearly, no structure assignment can be made for this sample but likely peak regions have been highlighted; this map is representative of the entire set. This is in contrast to the maps obtained for SWNT dispersed in SDBS showing strong emission peaks, the strongest of these is given in Figure 11 while Figure 12 gives the map from a high concentration sample, with (n, m) indices assigned where possible. Comparing Figure 10 and Figure 11, it is possible to assert that the circled zones would show defined peaks if the intensity was improved. This could be achieved by using a summation from two or more maps – this was not possible for this study as there was insufficient liquid nitrogen capacity in the dewar.

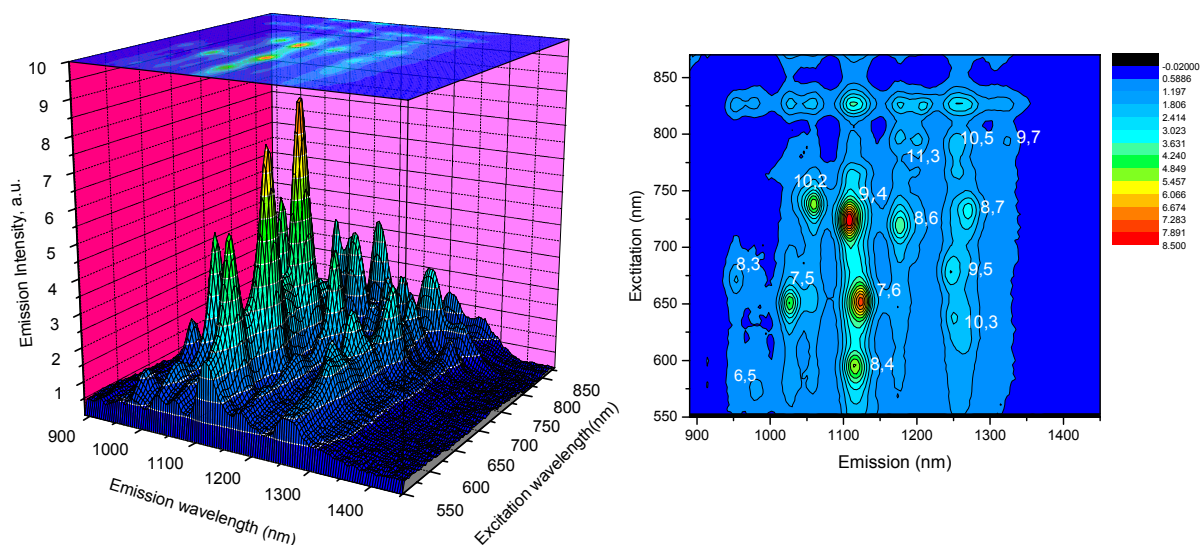


Figure 11: PL map SWNT in SDBS, Sample E (0.029 mg/mL).

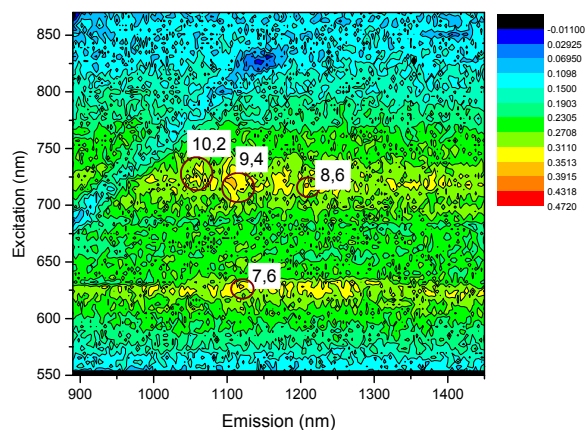


Figure 12: PL map SWNT in SDBS, Sample B (0.185 mg/mL).

The higher concentration SDBS sample clearly has significant quenching of the nanotube fluorescence. The peaks that are barely discernable in Figure 12 correspond to the strongest peaks in Figure 11. This was expected at high concentration as there is significant bundling of the nanotubes with photons emitted from transitions in semiconducting tubes being absorbed by adjacent metallic tubes.

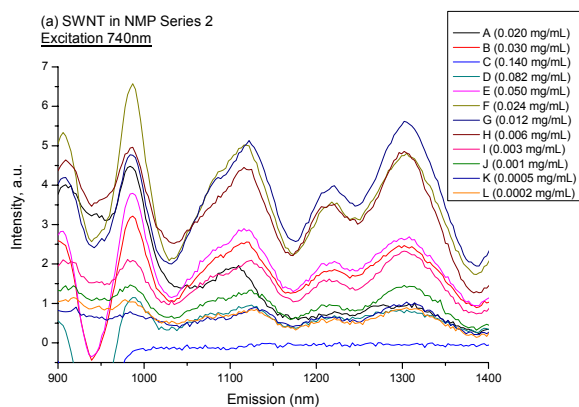


Figure 13: NIR-PL line scans, SWNT in NMP.

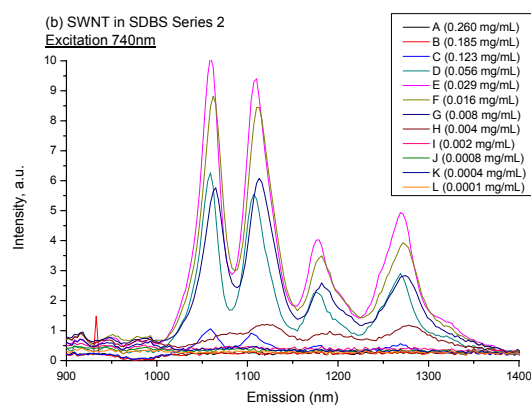


Figure 14: NIR-PL line scans, SWNT in SDBS.

In order to assess nanotube population as a function of concentration, line scans were taken where a large number of strong peaks were observed (a 740 nm excitation was chosen); these are given in Figure 13 and Figure 14 above. The relatively wider peaks in NMP can be partly attributed to the widening of the monochromator widths; some effect from the nature of the NMP solvent is expected and, in addition, others have reported slight redshifting of peak positions compared to D₂O/surfactant dispersions¹⁷. While the overall incident light intensity may have been slightly increased, the peak amplitude is still observed to be lower than that from the SDBS dispersions; the taking of a summation of three or more repeat line scans would be expected to improve the resolution. The shapes of the above spectra were unchanged with concentration and so the intensity was proportional to the number density of individual nanotubes in the samples ($I_{PL} \propto N_{ind}/V$). To better assess the concentration dependence of the photoluminescence, the intensities at selected emission peaks were taken, and these were also divided by the nanotube concentration, C_{NT} . The concentration normalised values will be discussed further in the context of the AFM analysis of the bundle distributions. These plots are given below in Figure 15 and Figure 16.

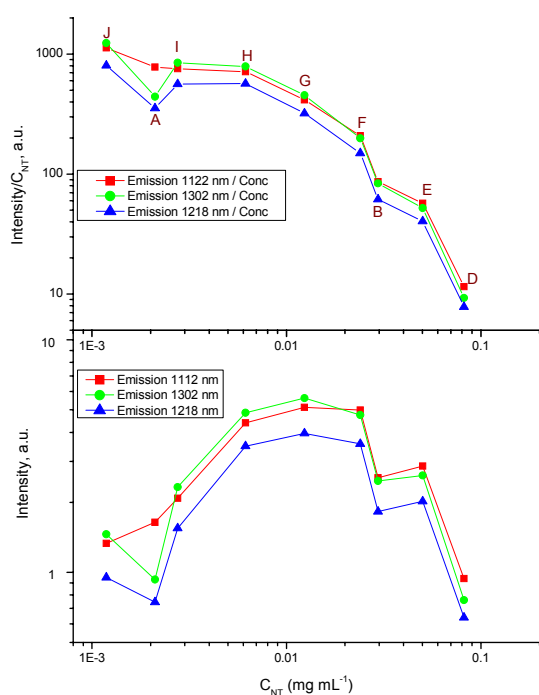


Figure 15: PL line scan intensities, SWNT in NMP.

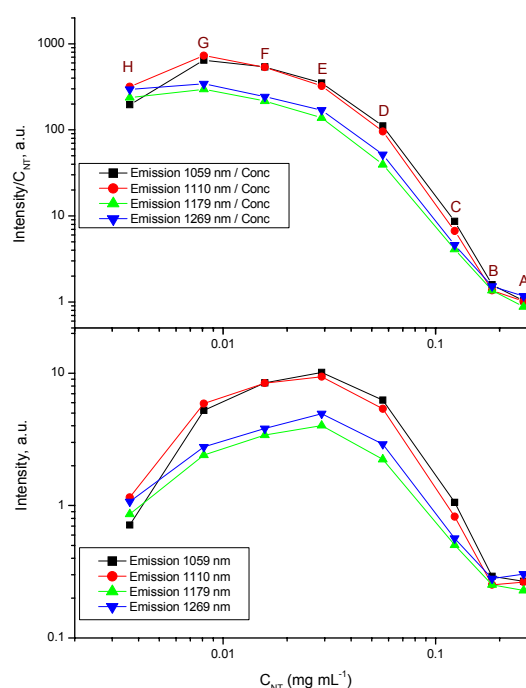


Figure 16: PL line scan intensities, SWNT in SDBS.

For the NMP sample, the peak around 980 nm was disregarded as it is unclear that it is a true nanotube emission; this assertion was based on the full excitation-emission map Figure 10, and by comparison to the SDBS peak positions. Of note in Figure 15 is the dip in both intensity and concentration-normalised intensity for samples A and B. This is an expected result as these samples were at the highest initial concentration with the centrifugation process removing most of the material present. This material would have been in the form of large aggregates and the PL data suggests that the remaining nanotubes were in the form of large bundles, relative similar final

concentrations. Without the use of an additional sonication after centrifugation, it is likely that these bundles did not break up, thus resulting in a relatively reduced PL intensity. This effect is not seen in the SDBS dispersions with a more smooth progression in intensity. Both datasets show a peak in emission intensity at intermediate concentrations between 0.009 and 0.012 mg/mL, indicating that these concentrations maximise the number density of individual nanotubes. For the NMP system, the normalised intensity is seen to rise slowly with decreasing concentration while a dip is observed in the SDBS system. As a point of caution, it is stressed that the coupling of a low PL intensity and error in C_{NT} at low concentrations may give unreliable trends. However, taking the trends at face value, they may suggest that the mass fraction of individual tubes rises with reducing total concentration in NMP, indicating better debundling. For the given SDBS system, Figure 16 indicates a dip in M_{ind}/M_{tot} at low concentration, perhaps suggesting that some rebundling is taking place.

To better examine the distribution of individual nanotubes AFM analysis was used. Samples were deposited as described earlier and all data was derived from 10.0 μm square scans. To determine the diameter of the tubes observed, the z-height of flattened images was used; lateral measurements would have to account for the effect of tip radius which was approx 50 nm for the Si tips used. For length analysis, this inherent error was neglected as typical objects measured were of the order of 1 μm . A small area scan for an NMP sample at low final concentration is given below. In addition, a collection of HR-TEM images of NMP dispersion dropped on holey carbon grids are given in Figure 18. Further sample AFM scans for NMP and SDBS sample are given in Appendices 4.01 and 4.02, respectively.

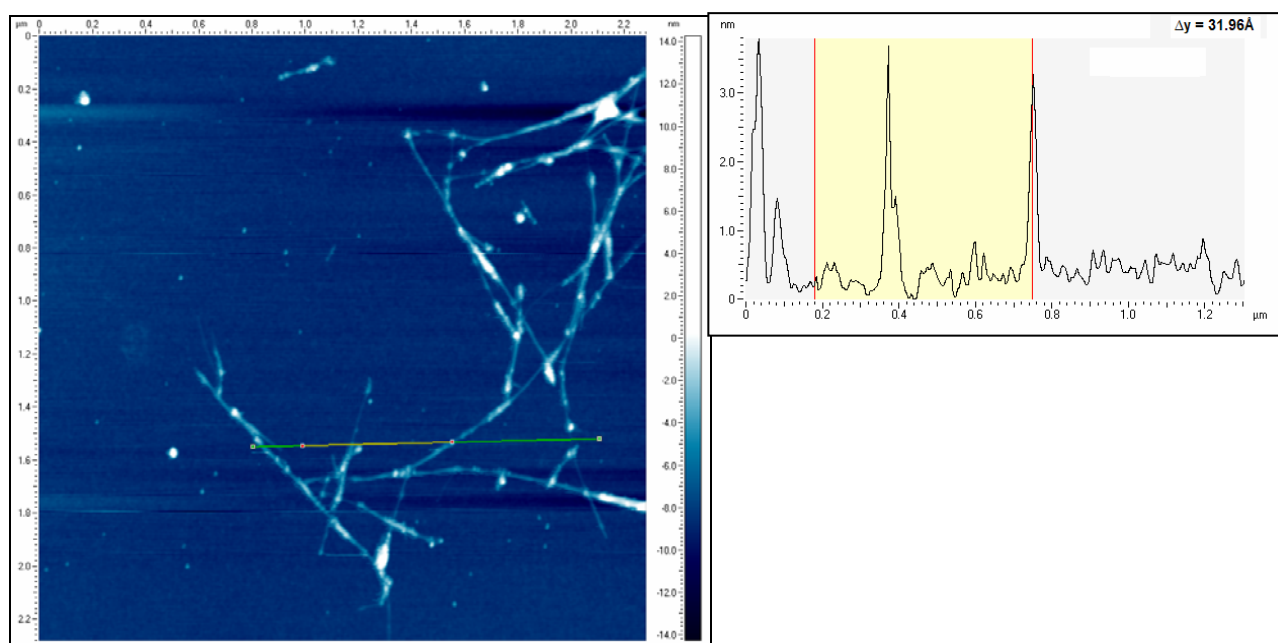


Figure 17: AFM scan, SWNT in NMP sample I (0.003 mg/mL).

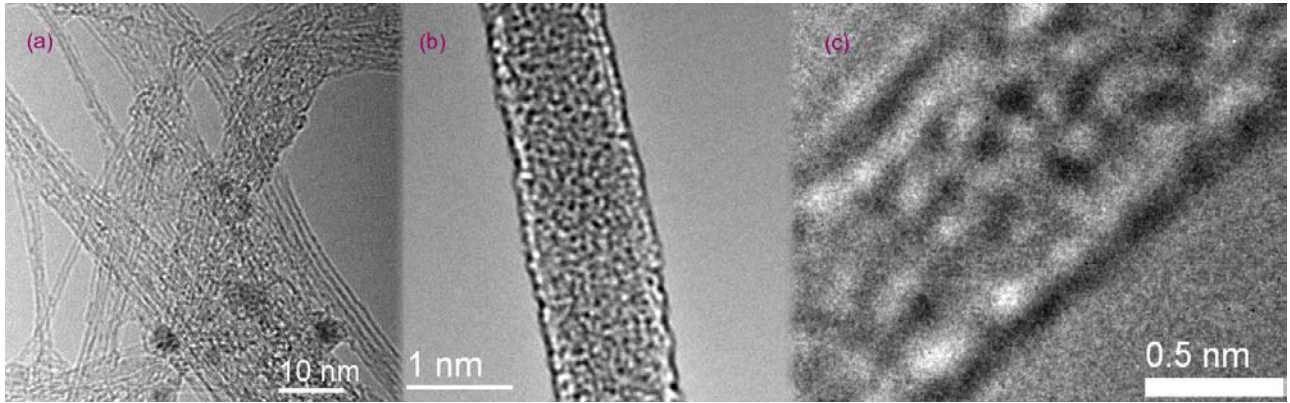


Figure 18: HR-TEM images, (a) high concentration bundles (sample C 0.140mg/mL), (b) and (c) individual nanotubes at low concentration. Images courtesy of *****, School of Physics, TCD.

Diameter statistics were derived using 160 height measurements per concentration. HiPCO SWNT nanotubes are known to be produced within the diameter range 0.4 – 1.4 nm. Thus, species with heights < 1.4 nm are likely to be individual nanotubes, though the possibility remains that they are very small bundles composed of two or three narrow diameter tubes. Reliable length measurements were much harder to obtain due to nanotube entanglement and difficulty in determining tube or bundle end points; thus, 30 length measurements with corresponding mean diameters were taken per sample.

For SDBS dispersions there was the added complication of residual surfactant and the difficulty in avoiding drying effects. The drop cast method on heated silicon described earlier appeared to avoid this problem. We suggest that insufficient time was given for the nanotubes to re-arrange because the water was rapidly removed by evaporation. Further support for the efficacy of this method lies in the fact that a significant population of individual nanotubes were observed at all concentrations (see Figure 20 and Figure 22) – these species would be expected to re-bundle first as they are isolated species with the highest overall surface energy. In conducting the AFM counting, it was observed that there were lumps of surfactant remaining (upto 30 nm in height) but these were usually easily identified and avoided as they did not typically cover the entire length of the tube (for images see Appendix 4.02, page 35).

Figure 19 and Figure 20 below present an overview of the diameter distributions for SWNTs in NMP and SDBS dispersions. Alternative graphical representations of the plots below are given by the histograms in Appendices 4.03 and 4.04. The histograms highlight the fact that significant populations of small bundles ($D < 2.5$ nm) were observed at all concentrations in NMP while the SDBS system showed populations of individual nanotubes ($D < 1.4$ nm) at all concentrations.

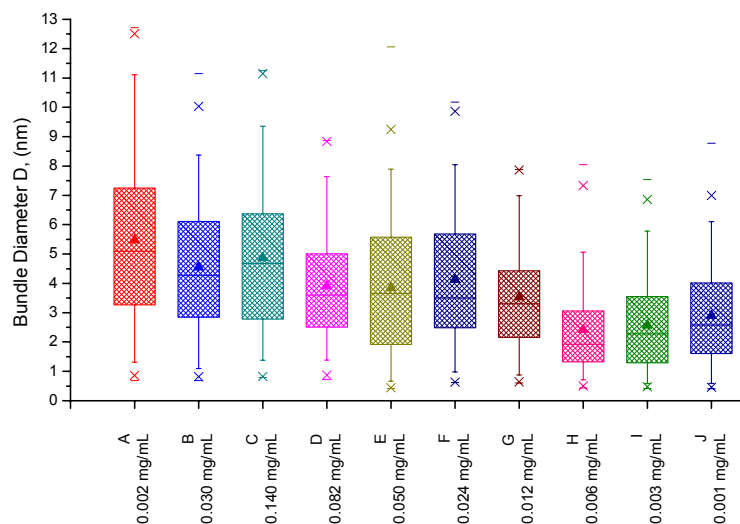


Figure 19: Diameter distribution box plots for NMP dispersions

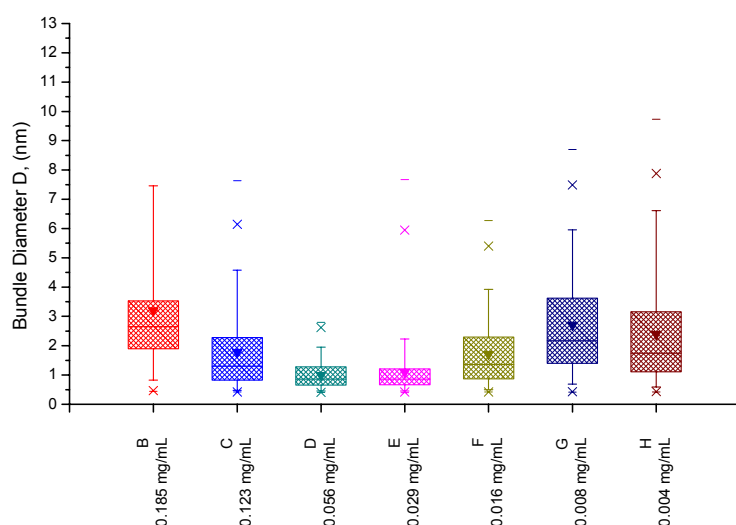


Figure 20: Diameter distribution box plots for SDBS dispersions

From these plots it is immediately apparent that the SDBS system yielded smaller bundles with a lower spread of diameters, compared to the NMP system. The SDBS system shows four concentrations (for samples C through F) where 75% of the nanotubes have bundle diameter less than 2.3 nm; in fact samples D and E have 75% of all species as individual tubes with diameter less than 1.3 nm. Also of note is that the highest initial concentration samples for NMP, A and B, have box plots that are similar to that of sample C. Both A and B were mostly composed of large aggregates that were removed by centrifugation; though the final concentrations of these samples was greatly reduced, Figure 19 suggests that the remaining nanotubes formed bundles with a diameter distribution more akin to a high final concentration.

To further examine the distribution, the root mean squared diameter and the number fraction of individual nanotubes were computed. The RMS diameter is easier to manipulate for the analysis to follow. The solid lines in Figure 21 and Figure 22 give fits for $D_{RMS} = \kappa\sqrt{C_{NT}}$ where κ is a constant, these fits will be used later.

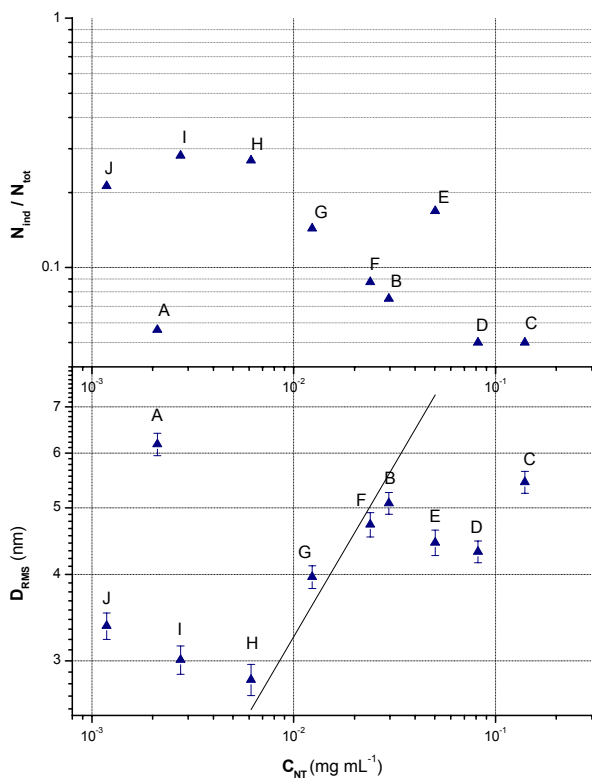


Figure 21: Diameter distribution analysis, SWNT in NMP.

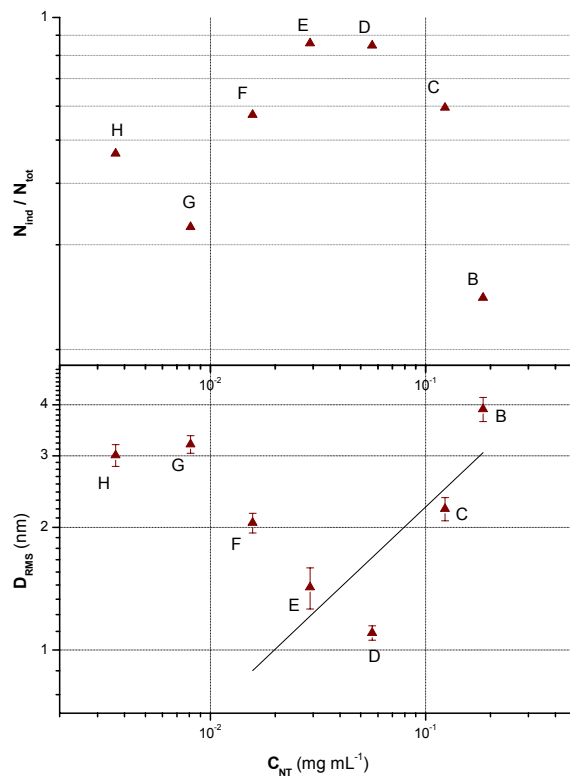


Figure 22: Diameter distribution analysis, SWNT in SDBS.

It is immediately clear that there is a significant behavioural difference between the NMP and surfactant systems. In general, the number fraction of individual nanotubes in NMP steadily rises as concentration is reduced, peaking around 30%. D_{RMS} is seen to be fairly constant at high concentration before falling off and then saturating, almost within error, to a value of around 3 nm. A similar saturation has been reported elsewhere^{17,27} and indicates that a small bundle size dominates at low concentration. The other reported saturation diameter of 2 nm is lower than that observed in this study but could be due to either a greater presence of water in our samples, slight variation in the sample preparation procedure or simply experimental error. Also, the high initial concentration samples, A and B, have number fractions and diameters that resemble high C_{NT} samples; this agrees with the earlier interpretation of Figure 19.

For the SDBS surfactant system, the number fraction of individual tubes peaks at around 83%, at an intermediate concentration, with lower values observed at *both* higher and lower concentrations. The variation of D_{RMS} with C_{NT} is in line with the number fraction trend, with minimum diameters at the intermediate concentrations (samples D and E). Comparing Figure 21 and Figure 22, it is clear that the surfactant system yielded much smaller bundles overall with much higher number fractions of individual nanotubes.

We can examine the debundling process more closely by considering the possibility that there is an equilibrium bundle number density. The presence of equilibrium would not be unreasonable as the effect of sonication to debundle the nanotubes will yield a system of

predominantly small bundles. This effect would be countered by re-aggregation, with the eventual establishment of a quasi-equilibrium.¹⁷ This equilibrium bundle number density, $(N/V)_{eq}$ can be written as follows

$$\left(\frac{N}{V}\right)_{eq} = \frac{C_{NT}}{\rho_{NT}\langle V_{bun} \rangle} \quad (4)$$

where ρ_{NT} is the nanotube density and $\langle V_{bun} \rangle$ is the average bundle volume at equilibrium. If we assume that all systems are at equilibrium following centrifugation, then the AFM data for length, with corresponding diameters, can be used to derive this average (mean) bundle volume as a function of concentration to ultimately yield the equilibrium number density.

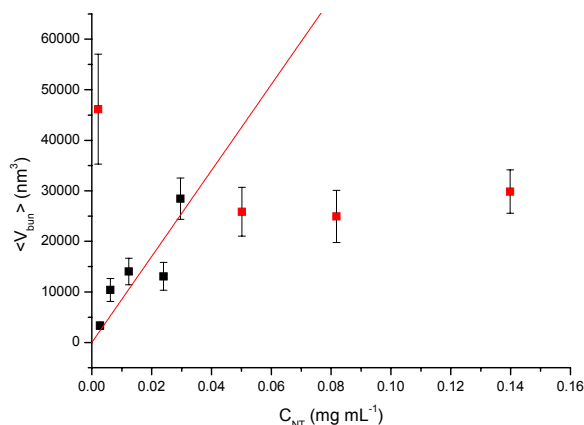


Figure 23: Mean bundle volume as a function of C_{NT} , SWNT dispersed in NMP

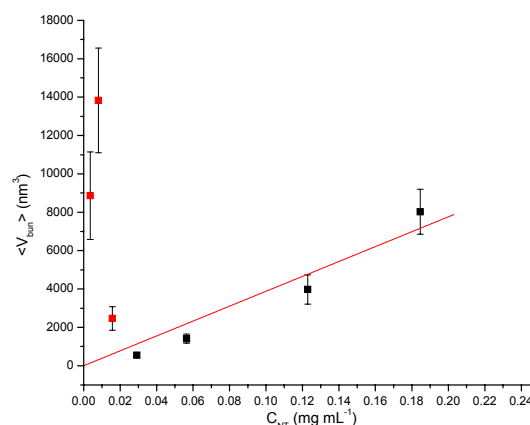


Figure 24: Mean bundle volume as a function of C_{NT} , SWNT dispersed in SDBS

In agreement with earlier results for diameter trends, the overall bundle volumes in SDBS are smaller than that those in NMP. In the case of the NMP system, the high concentration samples have fairly constant volume, within error, with a steady fall off as debundling begins. For the SDBS system, there is a minimum volume of about $540 \pm 100 \text{ nm}^3$ with a fairly linear fall off from high to low concentration (black points in Figure 24). The red lines in Figure 23 and Figure 24 are linear fits through the origin, with red datapoints omitted. Using the slopes of these lines and a nanotube density of 1500 kg m^{-3} , the value of $(N/V)_{eq}$ can be found. The inverse of $(N/V)_{eq}$ gives the equilibrium volume of solvent per bundle, $V_{solvent, eq}$.

Other research on NMP systems suggests that the bundle length is constant, within error, as a function of concentration.¹⁷ If this were the case for the systems in our study, the volumes from which the equilibrium parameters were derived may in fact be dominated by the diameter component. An analysis of the crude length distribution obtainable appears to show that bundles are longer than individual nanotubes. A plot of the variation of mean lengths of the bundles, $\langle L_{bun} \rangle$, and individual nanotubes, $\langle L_{ind} \rangle$, with concentration is given in Appendix 4.05, page 38. It is stressed that this comparison is limited by the size of the data sets. Only 13% of the NMP system's

length counts were of individual nanotubes ($D < 1.4$ nm) while the proportion was 40% for SDBS; this was expected due to the higher number fraction of individual nanotubes indicated by the diameter statistics. For the NMP dispersions, $\langle L_{ind} \rangle$, was 1.06 ± 0.08 μm while the overall average across all species regardless of diameter, $\langle L \rangle$, was 1.31 ± 0.05 μm . For SDBS dispersions, $\langle L_{ind} \rangle$ was 1.01 ± 0.05 μm and $\langle L \rangle$ was 1.11 ± 0.07 μm . The individual nanotube mean lengths agree within error and the higher value for overall length in NMP may be due to the lower proportion of individual nanotubes present (if in fact the bundled species are longer). Figure 25 below gives the concentration variation of the mean lengths, taken across all lengths measured, regardless of diameter. Each data point represents the mean value from thirty separate length measurements (note that the error bars for longer lengths are exaggerated by the logarithmic scale).

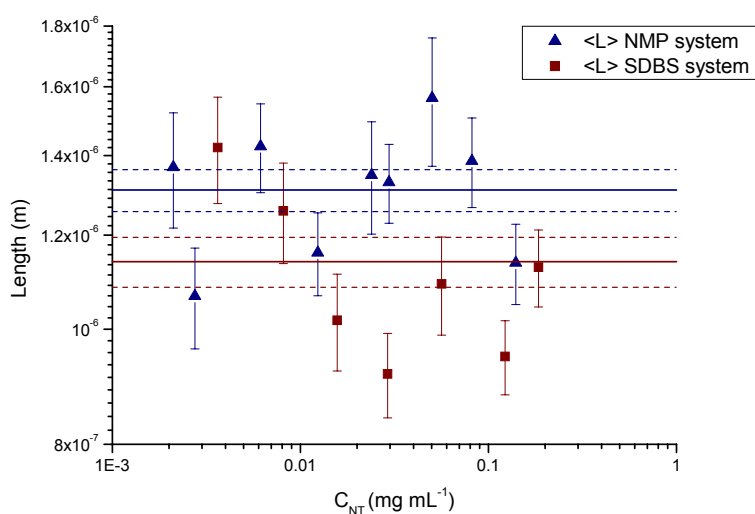


Figure 25: Mean nanotube bundle (including individual) lengths as a function of concentration. Solid horizontal lines give overall mean values with standard error limits (dashed lines).

The NMP dataset indicates that the overall length is approximately invariant with concentration. The SDBS system, on the other hand, shows a defined 54% increase in length from 0.92 ± 0.08 μm to 1.42 ± 0.15 μm over the range of the lowest four concentrations. Setting aside the impact of populations of bundles and individuals in the sample, this is a significant difference that would suggest that the bundle volume change with concentration is not simply a feature of the diameter distribution. Such a variation in bundle length may indicate true concentration dependence as has been shown for the bundle diameter. However, from the statistics available in this study, and the limitations therein, we cannot say this with certainty. It may be that case that the bundles do have a tendency to maximise contact area but that as bundle diameter increases, the probability increases that an imperfect alignment occurs with individual tubes sticking out of the bundles; this would explain why the trend in the SDBS system at the lowest concentrations is qualitatively in line with the trend in increasing bundle diameter in Figure 22.

Due to the low sample size it is not possible to give a definitive result and so the possibility that the lengths of individuals and bundle are equal must be considered. Due to the uncertainty, the remaining analysis will use the overall mean lengths, $\langle L \rangle$; this has the advantage of allowing the use of the D_{RMS} dataset, which was a bigger dataset obtained with much lower errors, to compute volumes. Under this assumption we can derive again the equilibrium number density of bundles. Modifying eqn 4 by substituting the average bundle volume gives:

$$\left(\frac{N}{V}\right)_{eq} \approx \frac{C_{NT}}{\rho_{NT}\pi\langle L\rangle\sqrt{\langle D^2\rangle}} \quad (5)$$

$$\Rightarrow D_{RMS} \approx \kappa\sqrt{C_{NT}} \text{ where } \kappa = \left(\frac{(V/N)_{eq}}{\rho_{NT}\pi\langle L\rangle}\right)^{\frac{1}{2}}$$

This eqn has been fitted to Figure 21 and Figure 22, page 22, and represents a good fit for the NMP system and a reasonable fit for the SDBS system. The results derived are presented below in Table 1, alongside the earlier results from bundle volume information.

		NMP dispersion	SDBS dispersion
$\langle L \rangle$		$1.31 \pm 0.05 \mu\text{m}$	$1.11 \pm 0.07 \mu\text{m}$
$(N/V)_{eq}$	Using AFM volume data	$7.9 (\pm 1.2) \times 10^{17} \text{ m}^{-3}$	$1.7 (\pm 0.2) \times 10^{19} \text{ m}^{-3}$
	Assuming constant length	$6.5 (\pm 0.9) \times 10^{17} \text{ m}^{-3}$	$4.8 (\pm 2.4) \times 10^{18} \text{ m}^{-3}$
$V_{solvent, eq}$	Using AFM volume data	$1.3 (\pm 0.2) \times 10^{-18} \text{ m}^3$	$5.9 (\pm 0.6) \times 10^{-20} \text{ m}^3$
	Assuming constant length	$1.5 (\pm 0.2) \times 10^{-18} \text{ m}^3$	$2.1 (\pm 1.0) \times 10^{-19} \text{ m}^3$

Table 1: Equilibrium nanotube lengths, bundle number densities and solvent volume per bundle

There is reasonable agreement, within error, between values derived based on the different approaches. We can draw further inference into the nature of the debundling in these systems by comparing the equilibrium volume of solvent per species (bundle or individual) to the volume of a sphere defined by $\langle L \rangle$. For the NMP system V_{sphere} had a value of $9.4 \pm 1.1 \times 10^{-18} \text{ m}^3$ while for the SDBS dispersion, the value was $5.8 \pm 1.1 \times 10^{-18} \text{ m}^3$. This V_{sphere} can be related to the concept of pervaded volume, more commonly used when discussing polymers.¹⁷ Comparing to the data in the above table, it is clear that the nanotubes dispersed in both solvents have greater pervaded volumes than the equilibrium volume of solvent available to each bundle. This implies that collisions between bundles can occur more easily and so aid rebundling. In terms of magnitude, the value of $V_{solvent, eq}$ is of the same order of magnitude as V_{sphere} and so the terms can be considered as reasonably close. In the case of the SDBS dispersion, the value of $V_{solvent, eq}$ is up to two orders of magnitude smaller than V_{sphere} . This suggests one of two things. One possibility is that the individual nanotubes and bundles in this system will have a tendency to reaggregate, due to close proximity of other tubes and frequent collisions, and as such the system may be considered

unstable. The alternative explanation is that the SDBS surfactant promotes better exfoliation of the nanotubes from bundles and allows closer packing of nanotubes.

Expanding the analysis further, the number density of *individual* nanotubes can be computed by simply noting that

$$\frac{N_{ind}}{V} = \frac{N_{ind}}{N_{tot}} \cdot \frac{N_{tot}}{V} \quad (6)$$

where the value of N_{tot}/V can be replaced by the equilibrium number density given in eqn (5). We can also compute the mass fraction of individual nanotubes at a given concentration by taking sums of the masses of individual species and cancelling appropriate terms,

$$\frac{M_{ind}}{M_{tot}} = \frac{\sum \frac{\rho_{NT} \pi D_{ind}^2 L_{ind}}{4}}{\sum \frac{\rho_{NT} \pi D^2 L}{4}} \approx \frac{\sum D_{ind}^2}{\sum D} \quad (7)$$

As a further extension, this mass fraction yields the partial concentration of individual nanotubes; this is the mass of individual nanotubes per unit volume solvent calculated from

$$\frac{M_{ind}}{V} = \frac{M_{ind}}{M_{tot}} \cdot \frac{M_{tot}}{V} = \frac{M_{ind}}{M_{tot}} \cdot C_{NT} \quad (8)$$

Dividing M_{ind}/V by N_{ind}/V yields the mass of an individual nanotube. The results of these calculations are presented graphically, with error bars where calculable, in Figure 26 and Figure 27 below. Red horizontal dashed lines give the positions of $(N/V)_{eq}$, derived from eqn 5 and blue lines give values from AFM volume data (eqn 4). Previously presented data for the number fraction of individual nanotubes is included as a reference. In addition, the photoluminescence intensity is proportional to the number density of individual nanotubes. This in turn is related to the mass of individual nanotubes per unit volume by $\frac{N_{ind}}{V} = \frac{M_{ind}}{M_{NT}V}$, where M_{NT} is the nanotube molar mass.

Substituting eqn 8 shows that I_{PL}/C_{NT} is proportional to the mass fraction of individual nanotubes. The PL datapoints are derived from the earlier values of I_{PL} and I_{PL}/C_{NT} data presented in Figure 15 and Figure 16, page 18, and have been normalised to fit an intermediate concentration.

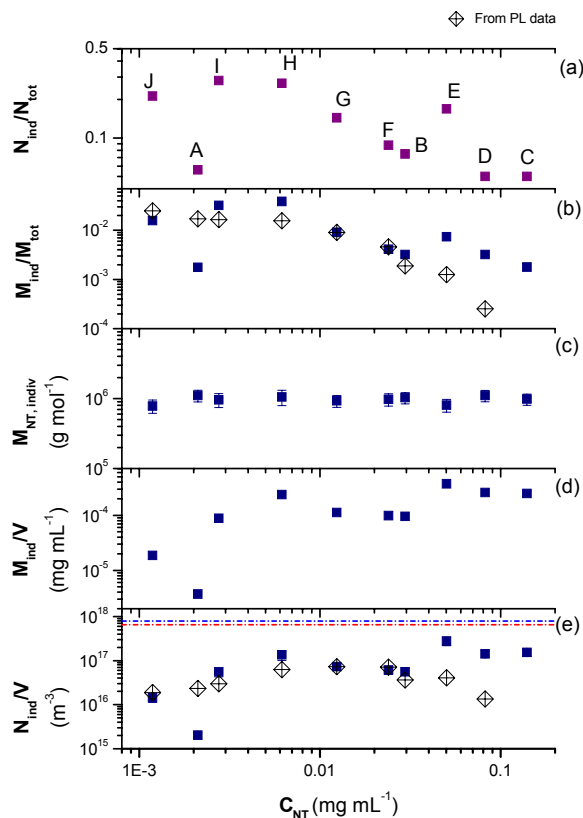


Figure 26: Parameters, derived from AFM and NIR-PL measurements, for individual SWNT dispersed in NMP as functions of concentration. (a) Number fraction. (b) Mass fraction. (c) Molar mass. (d) Partial concentration. (e) Number density.

From the above plots, it is shown that the nanotube molar mass is roughly constant with an average of the plotted values of $9.7 (\pm 0.4) \times 10^5$ g/mol from the NMP dataset and $7.0 (\pm 0.4) \times 10^5$ g/mol from the surfactant system. These values are close, within error, as expected as both dispersions were prepared from the same batch of raw CNT powder. For the NMP system, the data for M_{ind}/V , the partial concentration of individual nanotubes, suggests that there is an optimum concentration of 0.006 mg/mL; this is if one considers the high partial concentration at the high concentrations as erroneous. For the SDBS systems, the optimum concentration is much higher at 0.056 mg/mL.

Examining parts (b) of the above, it is clear that the mass fraction of individual nanotubes follows a similar trend to the number fraction. There is a slight disagreement with the PL information in both cases; the high concentrations in NMP have relatively lower mass fractions of individuals present than suggested by PL and similarly for the low concentrations in SDBS. The mismatch is repeated in the case of the number density of individual nanotubes, parts (e), though it must be remembered that there is an undetermined error in all these data points and so direct comparison may be unfair (in this context the overlap of PL and AFM data for the NMP samples can be considered good). For the SDBS system, it is clear that a significant discrepancy may exist.

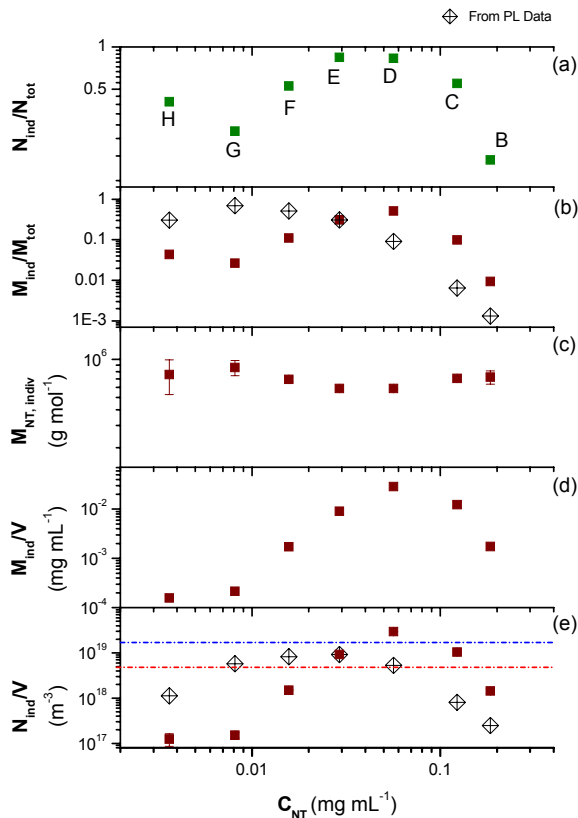


Figure 27: As per Figure 26 for individual SWNT dispersed in SDBS.

It may be the case that there is a time dependent rebundling effect that could potentially explain the trends. It has been suggested elsewhere that the individual nanotubes at low concentration in surfactant may re-bundle over time. In a low concentration environment, the surfactant molecules may desorb from the nanotube without being replaced and so tend the system towards larger bundle sizes.¹² In the case of NMP, other studies have suggested that the dispersions are stable for several weeks after sample preparation with no such rebundling effects.¹⁷ The experimental limitations of our study dictated that the AFM measurements were made one day after the PL in the case of the NMP samples and a three days after the PL scans for the SDBS system; in the latter case this may have been significant enough to change the bundle distribution significantly.

As a final note, the analysis of the DWNT dispersions in both NMP and SDBS was limited, possibly due to impurity material present in the raw powder (these nanotubes were purchased from Nanolab); this is a common feature of DWNT synthesis. It was observed that a large quantity of material precipitated out during centrifugation. The AFM images were unintelligible as the nanotube species were in large aggregated lumps, up to 50 nm in height with few well defined bundles or individual species. For completeness, the initial concentration analysis based on UV-vis absorption spectra is included in Appendices 5.01 and 5.02. It can be seen from these graphs that about 50% of the material initially sonicated was removed by centrifugation. An alternative batch of DWNT from Nanocyl yielded similar results for aggregate proportions in NMP to the Nanolab tubes. Due to experimental error, the low concentration samples showed erratic absorbance behaviour. However, the AFM deposition at a final concentration of 0.009 mg/mL clearly indicated the presence of very long species (around 4 μm) with diameters in the range 1 to 7 nm, albeit with large impurity lumps. Due to time limitations, it was not possible to repeat this analysis.

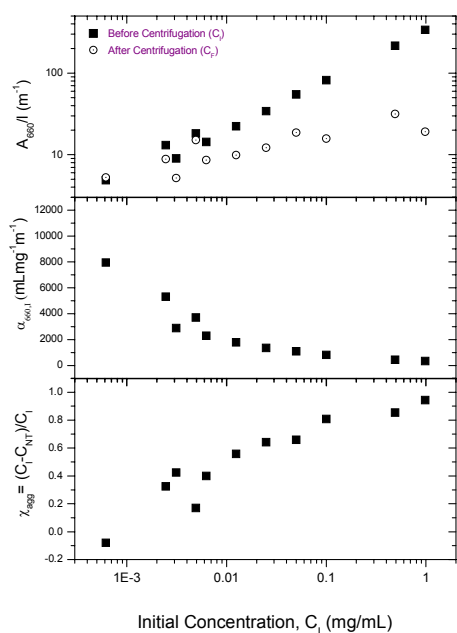


Figure 28: Nanocyl DWNT, UV-vis absorption analysis

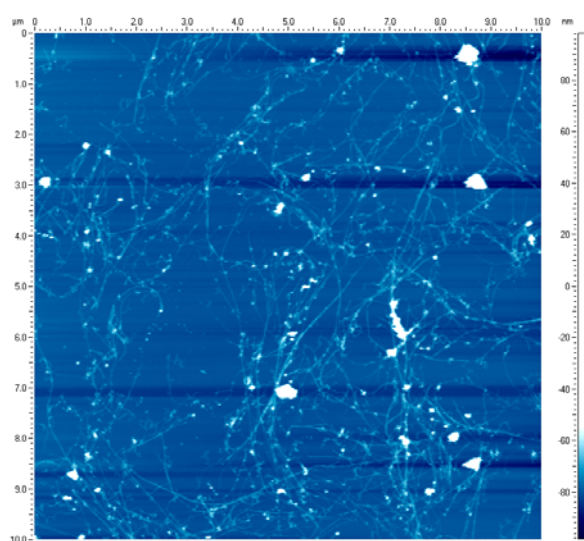


Figure 29: AFM image, Nanocyl DWNT (0.009 mg/mL)

Conclusions

In conclusion, good debundling resulting in large populations of individual single walled nanotubes is possible in both anionic surfactant and NMP dispersions. This is achievable using mild sonication and mild centrifugation (~ 3600 g). Probing the dispersions with UV-vis spectroscopy allows the proportion of large aggregates to be determined. To achieve good debundling of nanotubes, the SDBS system requires a greater input of acoustic energy to induce debundling compared to the NMP system; the distribution of nanotubes in SDBS, as indicated by the energy positions of direct band gap transitions, is not affected by an approximate six fold increase in sonication energy. In general, both dispersal systems have large aggregates at high concentrations, which are removed by the mild centrifugation. At intermediate concentrations, the mass fraction of large aggregates tends towards but does not reach zero. The very lowest concentrations appear to have an increase in aggregate concentration but this can be taken as an artefact caused by an increase in the pre-centrifugation extinction coefficient at these low concentrations; this rise may be attributable to a kinetically unstable fine dispersion of individual nanotubes immediately after sonication.

NIR-PL measurements on the surfactant system yield strong emission spectra and indicate large populations of individual nanotubes at all concentrations. PL intensity from the NMP systems is substantially weaker but relative populations of individual nanotubes are derivable. These fluorescence measurements indicate that the number density of individual nanotubes peaks at a concentration of 0.006 mg/mL in NMP and at 0.029 mg/mL in the surfactant; these maxima in number density suggest the existence of optimum initial concentrations of bundled nanotubes, for of the given amide solvent and surfactant ratio used. The PL data can be confirmed reasonably well by AFM measurements on drop-cast samples in the case of NMP but for the SDBS system, a deviation occurs at low concentration. It is suggested that the deviation is the result of a time dependent rebundling effect caused by irreversible desorption of the surfactant from the nanotube surface, under low concentration conditions.

AFM data shows that the bundle diameter saturates at about 3 nm at low concentration in NMP but displays a minimum value at an intermediate concentration in SDBS; this minimum RMS diameter in the surfactant is actually the size of an individual nanotube. It may be the case that there is also concentration dependence of bundle length in surfactant. This could be due to an increased probability of incomplete side to side overlap of the nanotubes as bundle diameter increases or could be a reflection of a dependence of overall bundle volume on concentration. AFM data also shows that the volume of solvent per bundle in NMP is lower, but of the same order of magnitude, than the volume of a sphere defined by the average bundle length. For the surfactant system, $V_{solvent, eq}$ is much lower and this may suggest that the surfactant system is

unstable with frequent collisions causing rebundling. It appears that the SDBS promotes good exfoliation of nanotubes during sonication and allows closer packing than the NMP dispersion medium, but that this system is less stable over time.

As an addendum, a brief outline of the authors views on future work related to this study is given in Appendix 6.03.

Appendix

Appendix 1

1.01 Structure Assignment of Optical Spectra

Below is a table reproduced from the paper by Bachilo et al.²¹ Symbols used are: λ for wavelength, h for Planck's constant, ν for frequency. λ_{22} and $h\nu_{22}$ refer to the wavelength and energy, respectively, for photon absorption between the second valence and second conduction band branches of the DOS. λ_{11} and $h\nu_{11}$ refer to the fluorescence emission transition between first conduction and first valence branches of the DOS.

λ_{11} (nm)	λ_{22} (nm)	$h\nu_{11}$ (eV)	$h\nu_{22}$ (eV)	Assignment
833	483	1.488	2.567	(5,4)
873	581	1.420	2.134	(6,4)
912	693	1.359	1.789	(9,1)
952	663	1.302	1.870	(8,3)
975	567	1.272	2.187	(6,5)
1023	644	1.212	1.925	(7,5)
1053	734	1.177	1.689	(10,2)
1101	720	1.126	1.722	(9,4)
1113	587	1.114	2.112	(8,4)
1122	647	1.105	1.916	(7,6)
1139	551	1.088	2.250	(9,2)
1171	797	1.059	1.556	(12,1)
1172	716	1.058	1.732	(8,6)
1197	792	1.036	1.565	(11,3)
1244	671	0.997	1.848	(9,5)
1250	633	0.992	1.959	(10,3)
1250	786	0.992	1.577	(10,5)
1263	611	0.982	2.029	(11,1)
1267	728	0.979	1.703	(8,7)
1307	859	0.949	1.443	(13,2)
1323	790	0.937	1.569	(9,7)
1342	857	0.924	1.447	(12,4)
1372	714	0.904	1.736	(11,4)
1376	685	0.901	1.810	(12,2)
1380	756	0.898	1.640	(10,6)
1397	858	0.887	1.445	(11,6)
1414	809	0.877	1.533	(9,8)
1425	927	0.870	1.337	(15,1)
1474	868	0.841	1.428	(10,8)
1485	928	0.835	1.336	(13,5)
1496	795	0.829	1.559	(12,5)
1497	760	0.828	1.631	(13,3)
1555	892	0.797	1.390	(10,9)

Table 2: Structure assignment of PL spectra

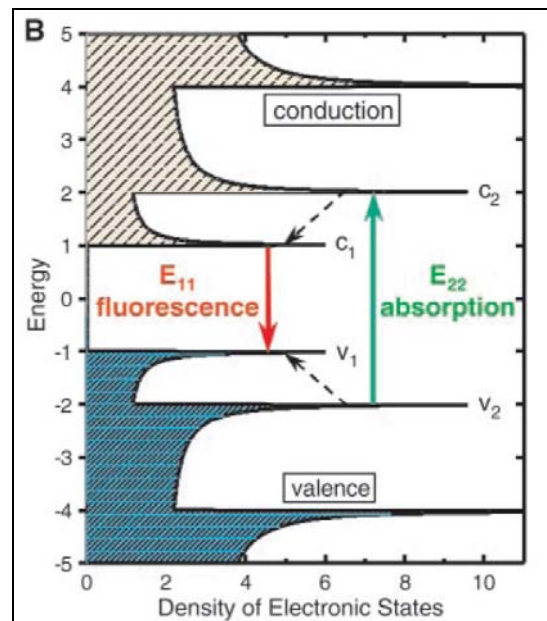
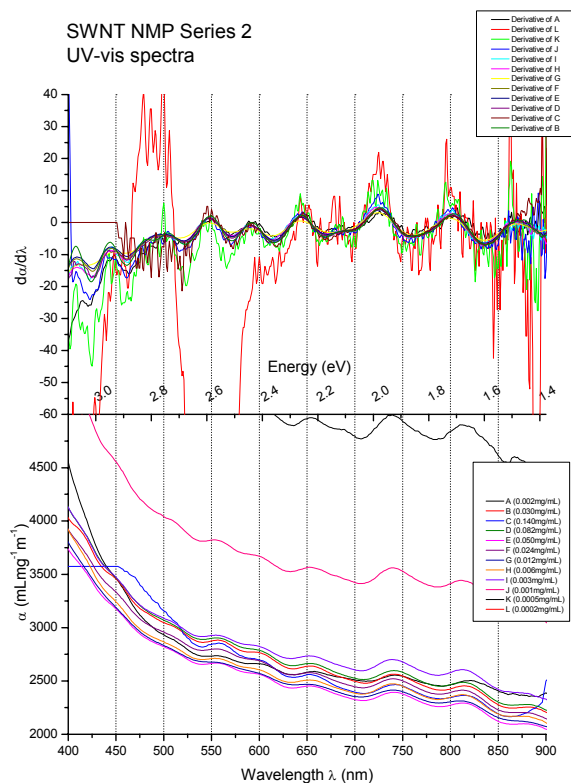


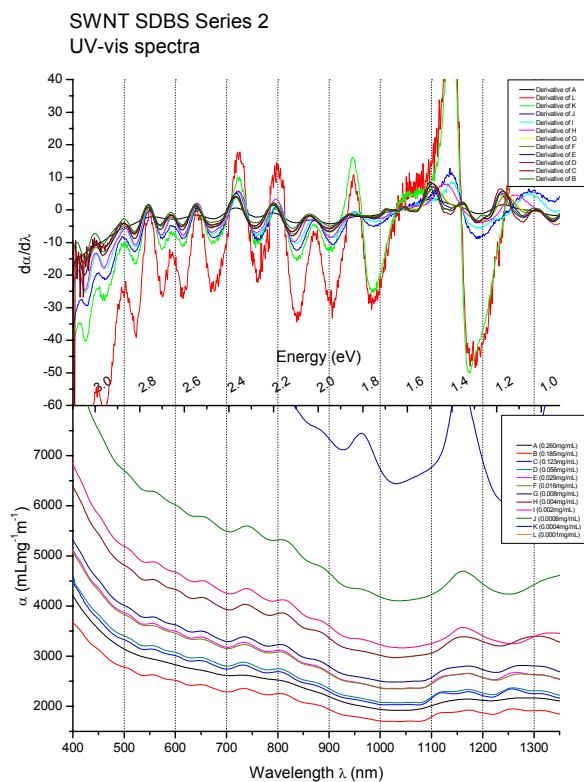
Figure 30: Illustrative band structure of SWNT

Appendix 2

2.01 SWNT in NMP, smoothed and differentiated UV-vis absorption spectra

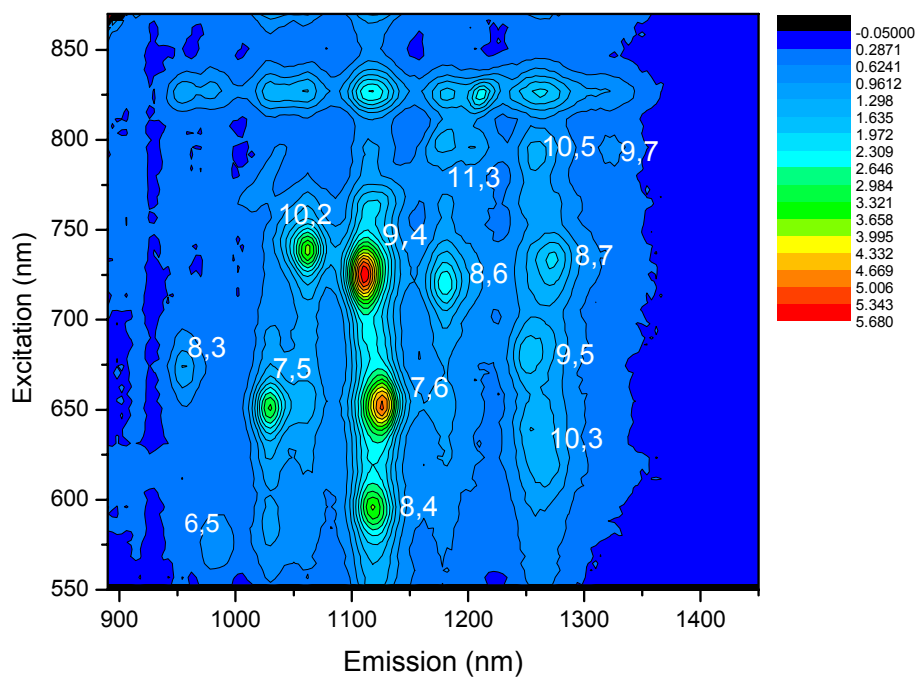
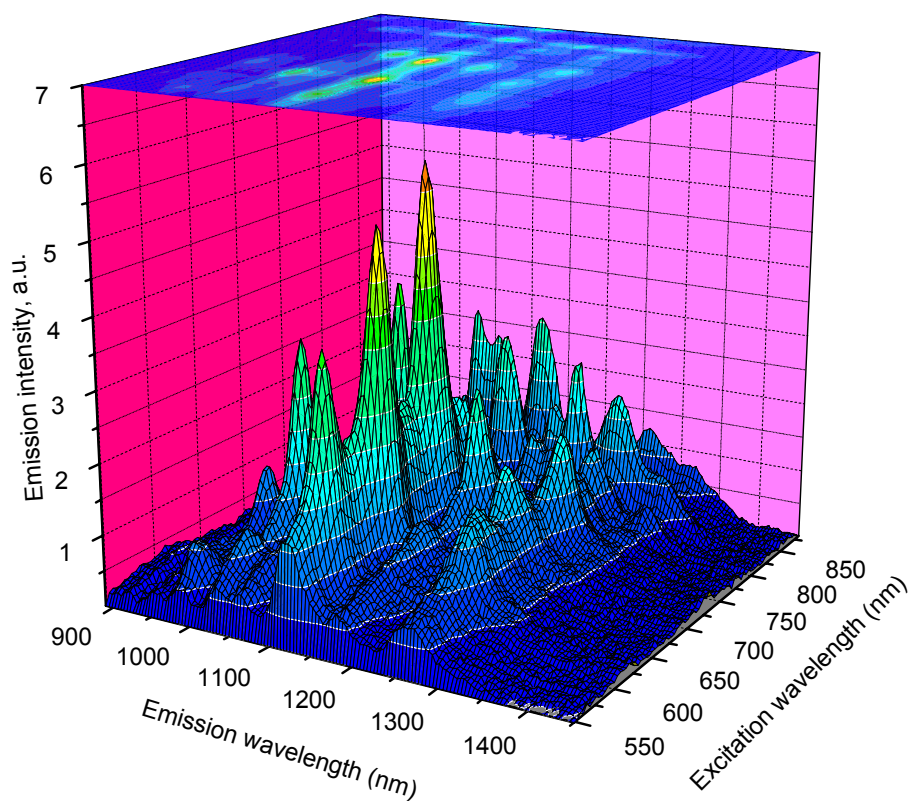


2.02 SWNT in SDBS, smoothed and differentiated UV-vis absorption spectra



Appendix 3

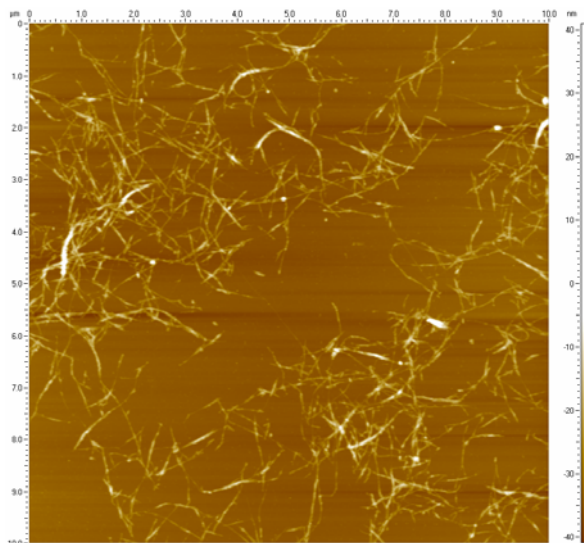
3.01 NIR-PL Map, SWNT in SDBS, Sample F (0.016 mg/mL)



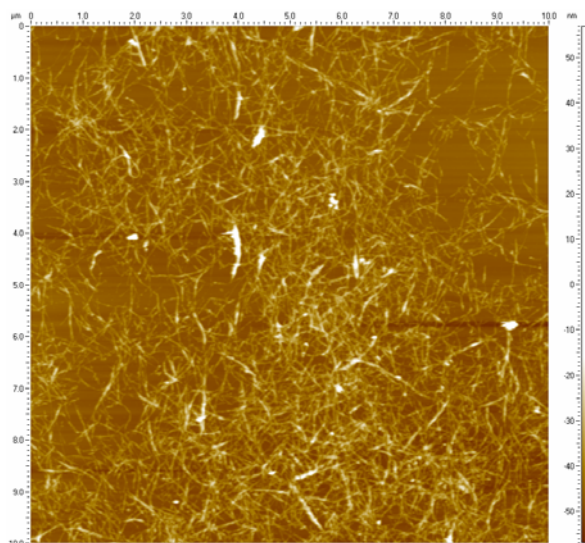
Appendix 4

4.01 AFM images, SWNT in NMP, series 2

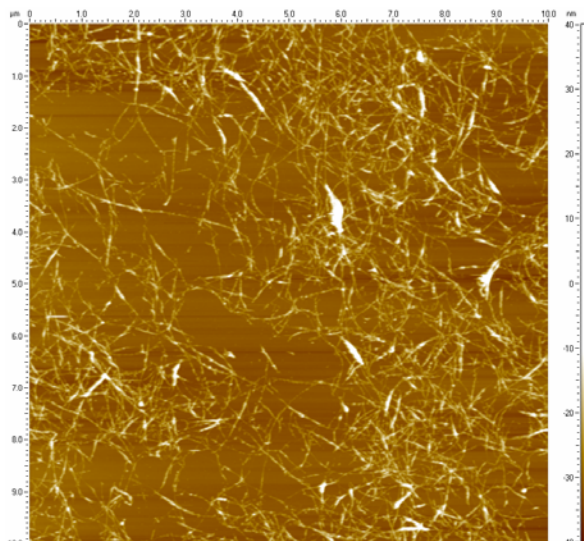
Sample A, 0.002 mg/mL



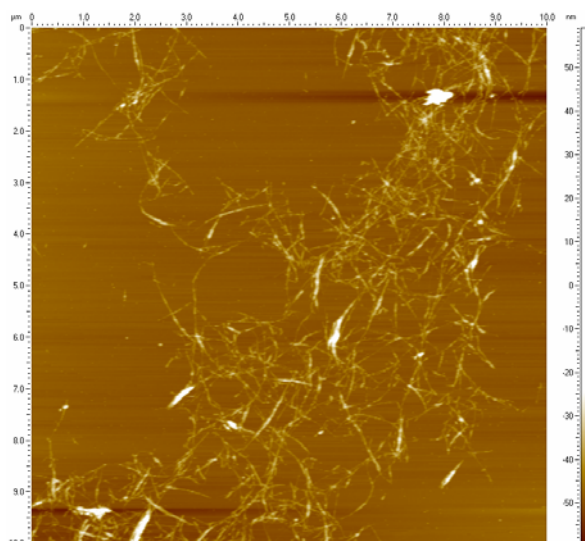
Sample C, 0.140 mg/mL



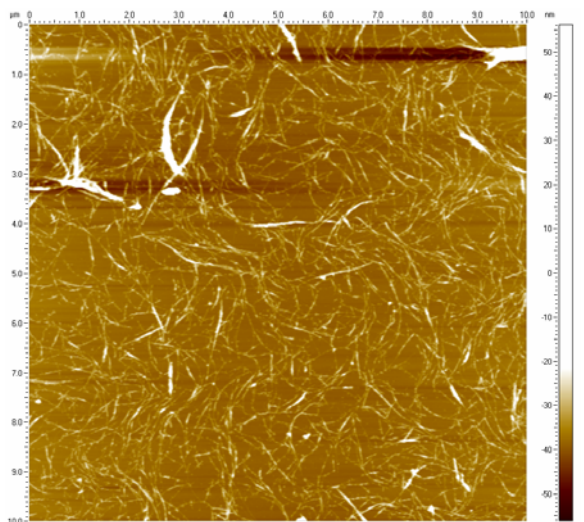
Sample E, 0.050 mg/mL



Sample G, 0.012 mg/mL

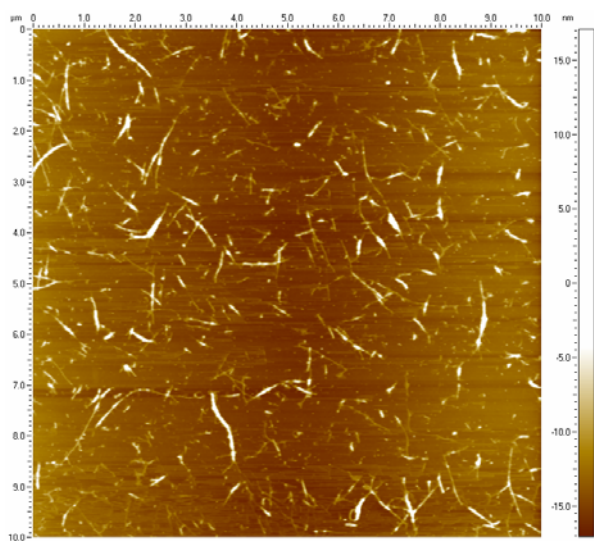


Sample J, 0.001 mg/mL

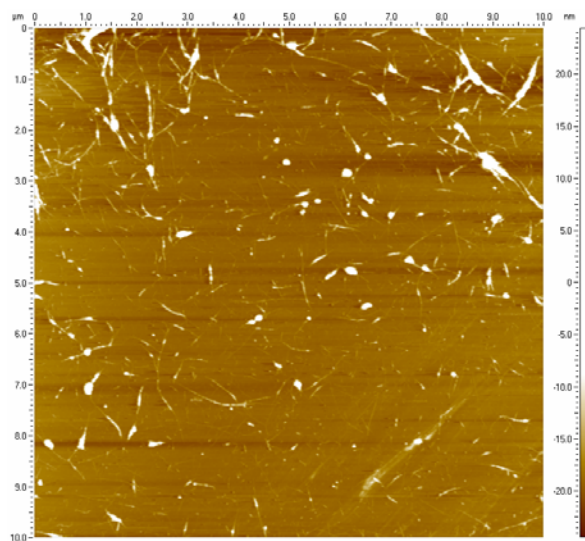


4.02 AFM images, SWNT in SDBS, series 2

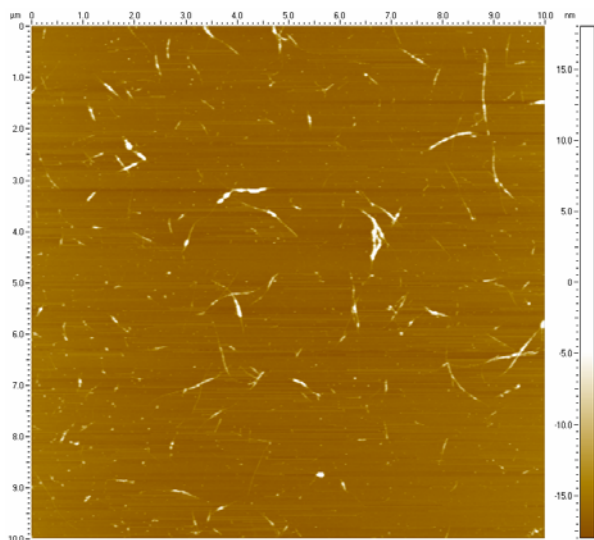
Sample B, 0.185 mg/mL



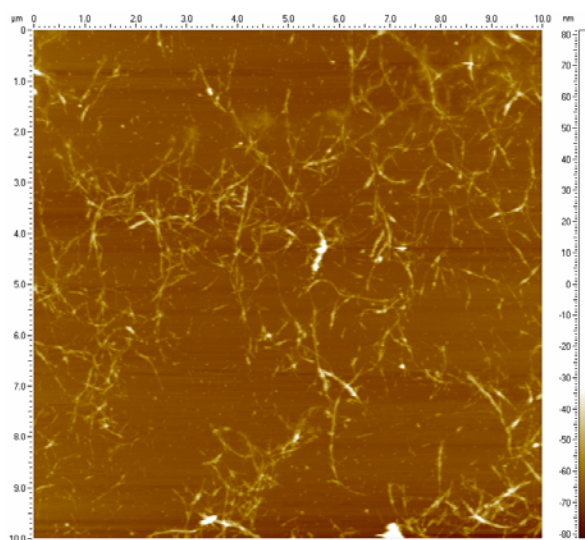
Sample D, 0.056 mg/mL



Sample F, 0.016 mg/mL

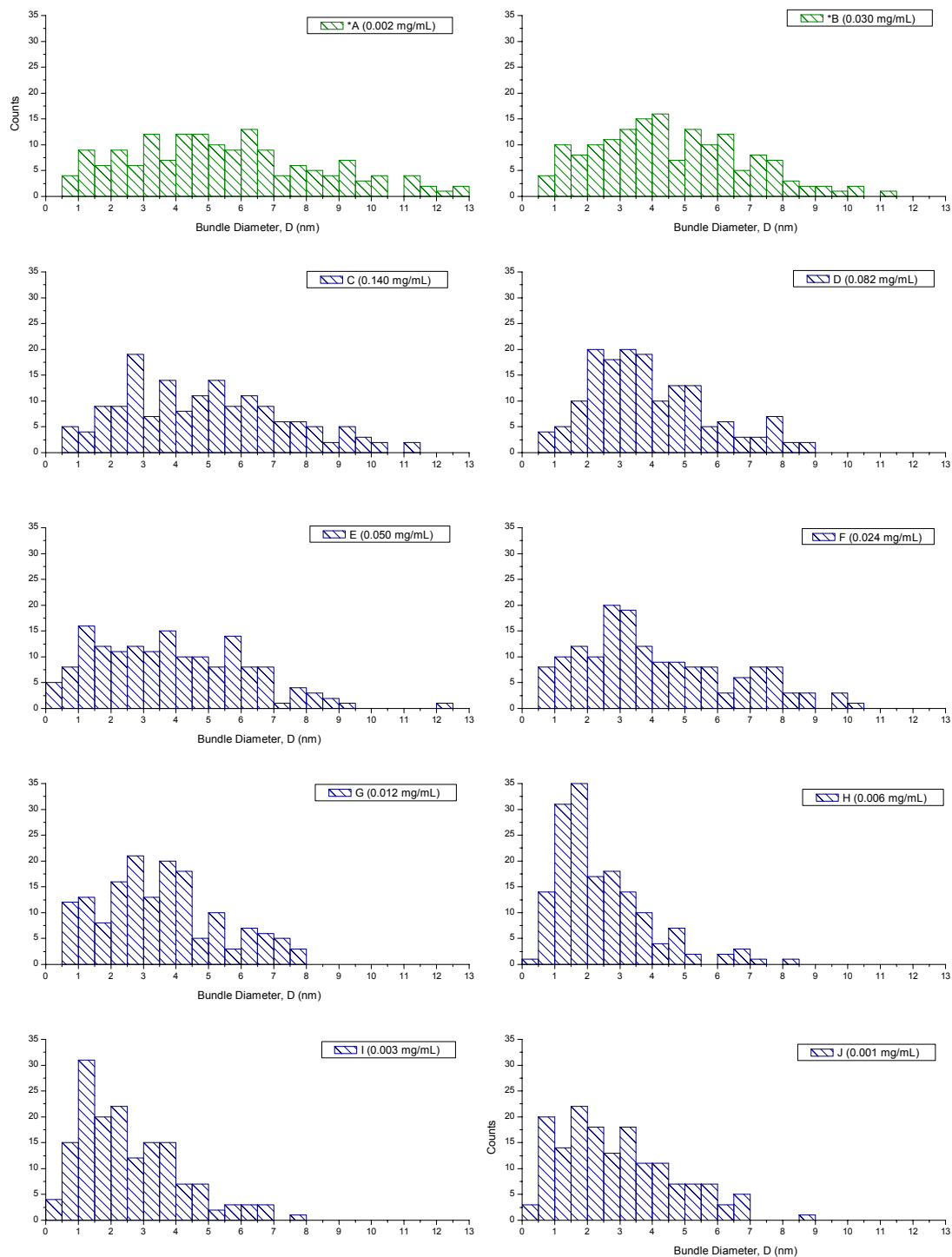


Sample G, 0.008 mg/mL

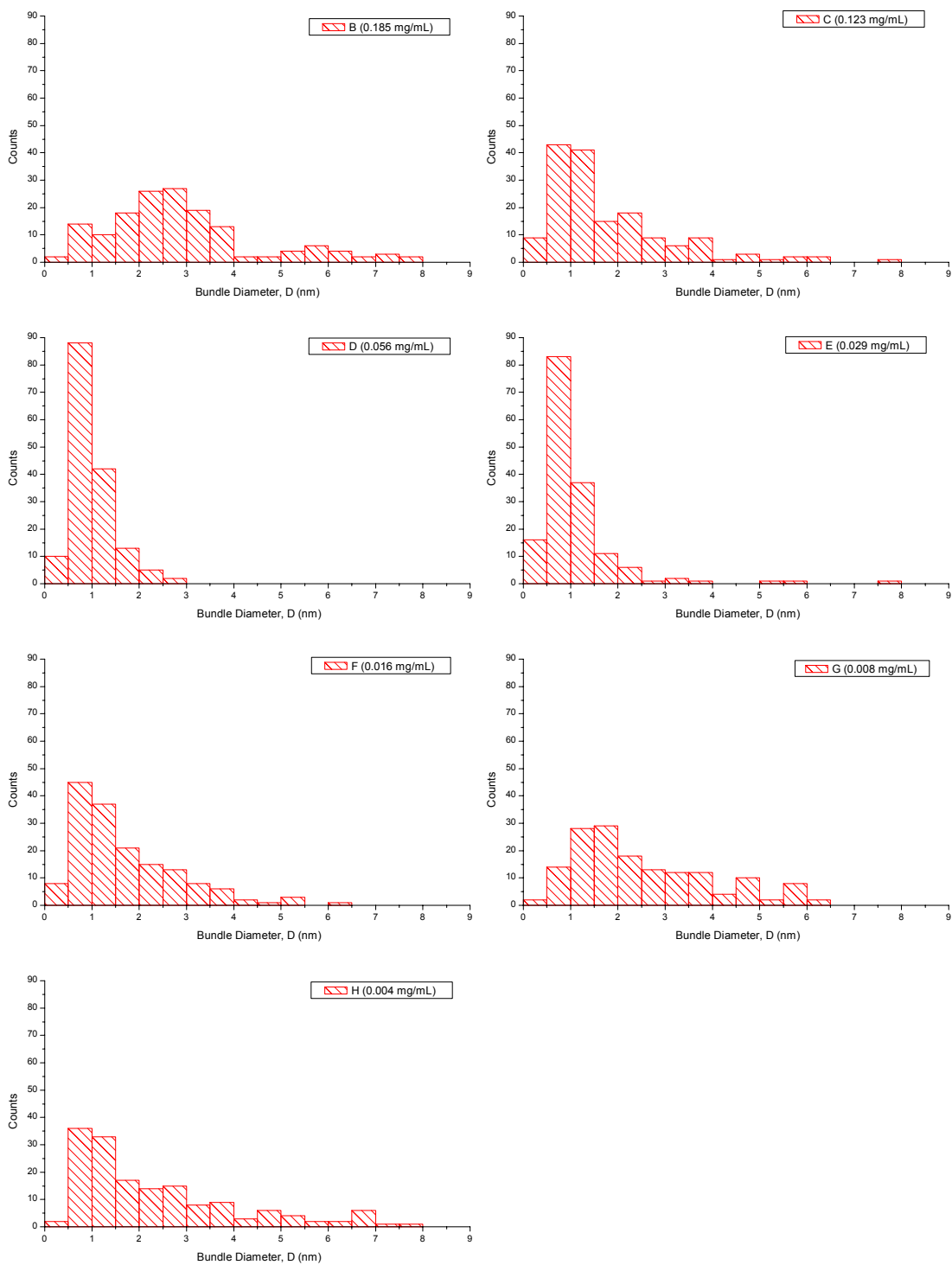


4.03 Histograms for bundle diameter change with concentration, SWNT in NMP

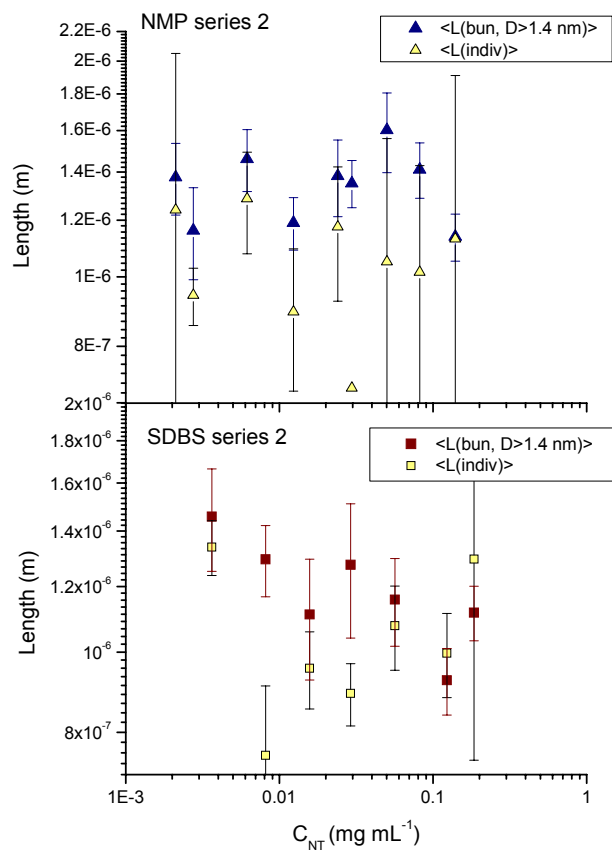
*Samples A and B started with highest initial concentrations



4.04 Histograms for bundle diameter change with concentration, SWNT in SDBS

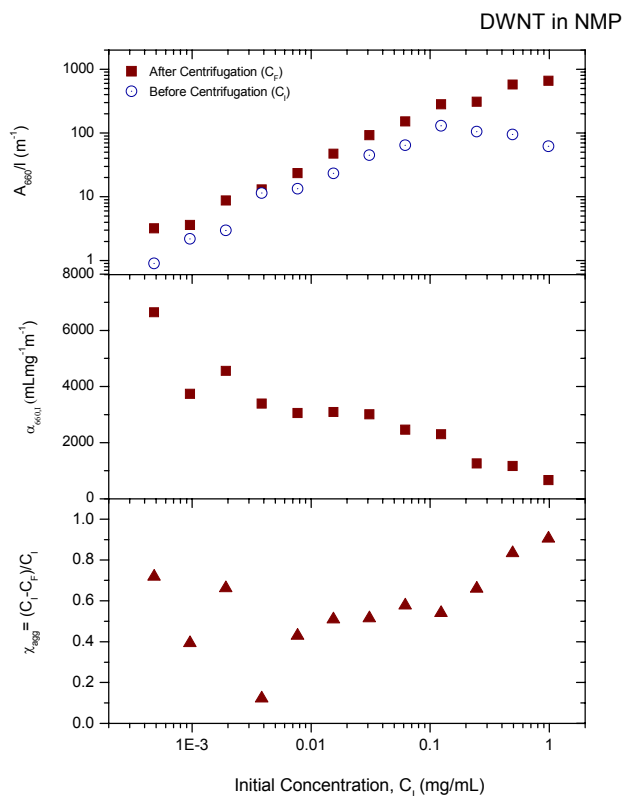


4.05 Individual and bundle mean nanotube lengths

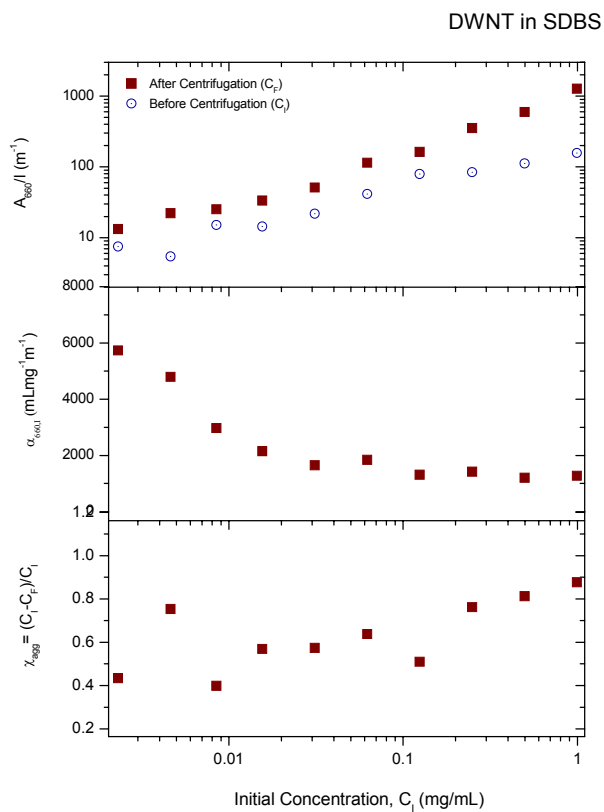


Appendix 5

5.01 DWNT in NMP concentration behaviour



5.02 DWNT in SDBS concentration behaviour



Appendix 6

6.03 Future Work

This study found that the dispersion of SWNT in SDBS yielded different results depending on the duration and overall energy input of the sonication process – a useful study would be to see the effect of wildly different sonication routines, including

- longer durations using point probe at 210W (to go beyond the intensity in this study)
- use of a horn tip with the use of larger sample volumes
- long duration low power sonication in bath

Details of the preparation procedure such as the volume of liquid in the sample vial, extent and temperature of cooling and the centrifugation speed need further investigation, in particular their effect on the population of individual nanotubes. Also of key importance is the issue of possible instability of individual nanotubes in SDBS which has a qualitative basis and some suggestive results from this study. What is needed is a kinetic PL assessment with results compiled across the range of concentrations. A related issue is that of the UV-vis absorption before centrifugation and the apparent rise in the extinction coefficient. This feature can be studied by preparing a low concentration sample, preferably using the serial dilution method to give an exact copy of procedure, and to analyse the change in UV-absorbance as a function of time (perhaps several hours). This would confirm the nature of the rise, be it a feature of equilibrium establishment in the dispersion or a systematic error that was carried across the majority of sample sets in this study (a similar analysis of the NMP system would also be instructive).

Obviously a significant extension to this study would be a full concentration dependence analysis of DWNTs in NMP and SDBS. The issue of the limitations of the PL machine in detecting emission from moderate to large nanotubes cannot be overcome readily but will not hinder an attempt out carry out AFM based analysis. The deposition methods for the SWNT in surfactant system could be transferred over to DWNT and comparison made. The issue of sample purity could possibly be addressed by more intense centrifugation, at the expense of yields.

References

1. Iijima, S. Helical microtubules of graphitic carbon. *Nature* **1991**, 354 (6348), 56-58.
2. Saito, R.; Fujita, M.; Dresselhaus, G.; Dresselhaus, M. S. Electronic-Structure of Graphene Tubules Based on C-60. *Physical Review B* **1992**, 46 (3), 1804-1811.
3. Dresselhaus, M. S.; Dresselhaus, G.; Jorio, A. Unusual properties and structure of carbonnanotubes. *Annual Review of Materials Research* **2004**, 34, 247-278.
4. Wong, E. W.; Sheehan, P. E.; Lieber, C. M. Nanobeam mechanics: Elasticity, strength, and toughness of nanorods and nanotubes. *Science* **1997**, 277 (5334), 1971-1975.
5. Ajayan, P. M.; Charlier, J. C.; Rinzler, A. G. Carbon Nanotubes: From Macromolecules to Nanotechnology. *Proceedings of the National Academy of Sciences of the United States of America* **1999**, 96 (25), 14199-14200.
6. Coleman, J. N.; Khan, U.; Blau, W. J.; Gun'ko, Y. K. Small but strong: A review of the mechanical properties of carbon nanotube-polymer composites. *Carbon* **2006**, 44 (9), 1624-1652.
7. Baughman, R. H.; Zakhidov, A. A.; de Heer, W. A. Carbon Nanotubes—the Route Toward Applications. *Science* **2002**, 297, 787-792.
8. Ryan, K. P.; Cadek, M.; Nicolosi, V.; Blond, D.; Ruether, M.; Armstrong, G.; Swan, H.; Fonseca, A.; Nagy, J. B.; Maser, W. K. Carbon nanotubes for reinforcement of plastics? A case study with poly(vinyl alcohol). *Composites Science and Technology* **6 A.D.**, *In Press, Corrected Proof*.
9. Kreupl, F.; Graham, A. P.; Duesberg, G. S.; Steinhogel, W.; Liebau, M.; Unger, E.; Honlein, W. Carbon nanotubes in interconnect applications. *Microelectronic Engineering* **2002**, 64 (1-4), 399-408.
10. Popov, V. N. Carbon nanotubes: properties and application. *Materials Science and Engineering: R: Reports* **2004**, 43 (3), 61-102.
11. O'Connell, M. J.; Bachilo, S. M.; Huffman, C. B.; Moore, V. C.; Strano, M. S.; Haroz, E. H.; Rialon, K. L.; Boul, P. J.; Noon, W. H.; Kittrell, C.; Ma, J.; Hauge, R. H.; Weisman, R. B.; Smalley, R. E. Band Gap Fluorescence from Individual Single-Walled Carbon Nanotubes. *Science* **2002**, 297, 593-596.
12. McDonald, T. J.; Engtrakul, C.; Jones, M.; Rumbles, G.; Heben, M. J. Kinetics of PL Quenching during Single-Walled Carbon Nanotube Rebundling and Diameter-Dependent Surfactant Interactions. *Journal of Physical Chemistry B* **2006**.
13. Yaws, C. L. *Chemical Properties Handbook*. McGraw Hill: 1999.
14. Duesberg, G. S.; Muster, J.; Byrne, H. J.; Roth, S.; Burghard, M. Towards processing of carbon nanotubes for technical applications. *Applied Physics A: Materials Science & Processing* **2004**, 69 (3), 269-274.
15. Heller, D. A.; Barone, P. W.; Strano, M. S. Sonication-induced changes in chiral distribution: A complication in the use of single-walled carbon nanotube fluorescence for determining species distribution. *Carbon* **2005**, 43 (3), 651-653.
16. Tan, Y. Q.; Resasco, D. E. Dispersion of single-walled carbon nanotubes of narrow diameter distribution. *Journal of Physical Chemistry B* **2005**, 109 (30), 14454-14460.

17. Giordani, S.; Bergin, S. D.; Nicolosi, V.; Lebedkin, S.; Kappes, M. M.; Blau, W. J.; Coleman, J. N. Debundling of Single-Walled Nanotubes by Dilution: Observation of Large Populations of Individual Nanotubes in Amide Solvent Dispersions. *J. Phys. Chem. B* **2006**.
18. Bonard, J. M.; Stora, T.; Salvétat, J. P.; Maier, F.; Stockli, T.; Duschl, C.; Forro, L.; deHeer, W. A.; Chatelain, A. Purification and size-selection of carbon nanotubes. *Advanced Materials* **1997**, *9* (10), 827-&.
19. Duesberg, G. S.; Muster, J.; Krstic, V.; Burghard, M.; Roth, S. Chromatographic size separation of single-wall carbon nanotubes. *Applied Physics A-Materials Science & Processing* **1998**, *67* (1), 117-119.
20. Landi, B. J.; Ruf, H. J.; Worman, J. J.; Raffaele, R. P. Effects of Alkyl Amide Solvents on the Dispersion of Single-Wall Carbon Nanotubes. *J. Phys. Chem. B* **2004**, *108*, 17089-17095.
21. Bachilo, S. M.; Strano, M. S.; Kittrell, C.; Hauge, R. H.; Smalley, R. E.; Weisman, R. B. Structure-Assigned Optical Spectra of Single-Walled Carbon Nanotubes. *Science* **2002**, *298*, 2361-2366.
22. Lian, Y.; Maeda, Y.; Wakahara, T.; Akasaka, T.; Kazaoui, S.; Minami, N.; Choi, N.; Tokumoto, H. Assignment of the Fine Structure in the Optical Absorption Spectra of Soluble Single-Walled Carbon Nanotubes. *Journal of Physical Chemistry B* **2003**, *107* (44), 12082-12087.
23. Maeda, Y.; Kimura, S.; Hirashima, Y.; Nagy, J. B. Dispersion of Single-Walled Carbon Nanotube Bundles in Nonaqueous Solution. *J. Phys. Chem. B* **2004**, *108*, 18395-18397.
24. Ausman, K. D.; Piner, R.; Lourie, O.; Ruoff, R. S.; Korobov, M. Organic solvent dispersions of single-walled carbon nanotubes: Toward solutions of pristine nanotubes. *Journal of Physical Chemistry B* **2000**, *104* (38), 8911-8915.
25. Furtado, C. A.; Kim, U. J.; Gutierrez, H. R.; Pan, L.; Dickey, E. C.; Eklund, P. C. Debundling and Dissolution of Single-Walled Carbon Nanotubes in Amide Solvents. *J. Am. Chem. Soc.* **2003**, *126*, 6095-6105.
26. Lisunova, M. O.; Lebovka, N. I.; Melezhyk, O. V.; Boiko, Y. P. Stability of the aqueous suspensions of nanotubes in the presence of nonionic surfactant. *Journal of Colloid and Interface Science* **2006**, *299* (2), 740-746.
27. Giordani, S.; Bergin, S.; Nicolosi, V.; Lebedkin, S.; Blau, W. J.; Coleman, J. N. Fabrication of stable dispersions containing up to 70% individual carbon nanotubes in a common organic solvent. *Physica Status Solidi B-Basic Solid State Physics* **2006**, *243* (13), 3058-3062.
28. Krupe, R.; Hennrich, F.; Hampe, O.; Kappes, M. M. Near Infrared Absorbance of Single-Walled Carbon Nanotubes Dispersed in Dimethylformamide. *J. Phys. Chem. B* **2003**, *107* (24), 5667-5669.